19

Application of Spatial-Analytical Tools and Current Climatic/Sea-level Models to Visualise the Changing Landscapes of Murujuga

THOMAS G. WHITLEY, MEGAN BERRY, LUCIA CLAYTON MARTINEZ

Developments in spatial-analytical and 3D photorealistic modelling tools provide us with the capacity to examine multiple terrain and palaeoenvironmental data sets and to create virtual interpretations of the landscape at various points in the past. These visualisations allow us to hypothesise about human settlement and land use as well as offering dramatic immersive or animated experiences. More importantly, visualised past environments are an insight into the cultural and sacred landscapes of Indigenous peoples, and may be useful tools for today's descendant communities to illustrate the significance of their heritage and find ways to manage and protect it from adverse future impacts.

Here we discuss application of these modelling tools to develop coastal terrain models at Murujuga over the last 125,000 years of environmental and shoreline change, to provide a basis for understanding human landscape use. We have combined data and analyses in ArcGIS 10.8.1 (Esri 2021) with the 3D visualisation platform of Terragen 4.5.7 (Planetside Software 2022). The objectives include:

- visualising the dynamics of sea-level change in the Dampier Archipelago (including Burrup Peninsula) over the last 125,000 years (i.e. the previous high-stand prior to the last glacial period through to today) to better understand the process of 'islandisation' and changing human access to coastal resources in the past;
- modelling the changes in vegetation types, densities and distributions across the landscape according to current knowledge of regional palaeoenvironmental and climatic indicators to give insight into patterns of early land use of Murujuga as attractors for settlement and rock art production through time;
- experimenting with digital spatial modelling technologies to apply different hydrodynamic and geomorphic scenarios, illustrating the complex notion of past 'shorelines' and how they may influence our models of human mobility and settlement;
- linking specific dated sites excavated at Murujuga (see McDonald et al. 2013, 2018b, and this volume) to visualise the palaeoenvironmental landscape at the time of their occupation;
- creating photorealistic representations of past landscapes with accurate vegetation types, densities and distributions, using low earth orbit, oblique aerial, near-ground and ground-level perspectives to provide immersive experiences keyed to specific sites at important time periods.

To achieve these objectives, we refined the terrain data and developed an overall process for converting both quantitative and qualitative data from various sources into visualisation and animation models (see Whitley et al. 2018 for the application of this approach to the broader North West Shelf). It should be stated at the outset that much of the data on which this modelling is predicated is at a regional scale and resolution. It is fragmentary, sometimes contradictory, and does not recognise local geological and hydrodynamic processes. Thus, while based on the most comprehensive information we currently possess, the results are strictly experimental. As more, and better, data becomes available, and particularly through ongoing research programs, these visualisations should become more locally applicable and informative.

Terrain Modelling

The base layer for this analysis is a terrain model derived from land above current mean sea level and that below it. These are defined in spatial-analytical terms as 'topography' and 'bathymetry' respectively. The accuracy of available terrain data varies across north-western Australia. When this project commenced (from 2015 to 2018) the initial Terragen modelling was based on the continent-wide Geoscience Australia (Whiteway 2009) raster data set at a resolution of 250 m (or 9 arc-seconds), which seamlessly merged topography and bathymetry. More detailed bathymetric data was available at 50 m resolution, but this was limited only to the transects for which multibeam scanning had been completed (Wilson et al. 2012). A 30 m (1 arc-second) hydrologically corrected digital elevation model (DEM) for the topography, ending at the shoreline and also from Geoscience Australia (Gallant et al. 2011), was utilised to replace the coarser terrain above modern sea level. This was data originally derived from the US NASA's Shuttle Radar Topography Mission (SRTM; see NASA 2022) and was hydrologically conditioned and drainage-enforced to match 1:250,000 scale watercourses.

A detailed high-resolution near-shore terrain model became available recently (Lebrec et al. 2021a) based on satellite images and 3D seismic surveys, integrated with historical depth soundings and referenced with open-source laser airborne depth sounder (LADS) and multi beam echo sounder (MBES) surveys. The resulting combined topography/bathymetry model has a 10 m resolution in near-shore areas and 30 m everywhere else. Vertical accuracy of the seismic data is better than 1 m + 2%, and the satellite data is better than 1 m + 5% of the absolute water depths (Lebrec et al. 2021a: 1). This publicly available data (Lebrec et al. 2021b) was used to rerun several of the Terragen models presented here.

At depths below –40 m, there is still a range of echo-sounding artefacts in the data resulting from differential substrate reflections, heave and roll, and water density at the time the various bathymetric surveys were conducted. Fourier transform techniques were applied in ArcGIS to decrease this data noise and interpolate a smoother surface. Fourier transform statistics average the depths across blocks of rasters and remove dramatic and repetitive fluctuations. In this case, a transform was applied across 1 km blocks of rasters, in areas where this effect was most severe. The result is a much smoother

surface which, although it loses some resolution, is a better approximation of the static bathymetry in those 'noisy' zones. The only real solution to this problem, though, is far more detailed physical data gathered at high resolution, correcting for error and water column or sea-floor interference.

Hydrologic Modelling

Topographic hydrology (i.e. water flow above sea level) has already been accurately mapped for the North West Shelf. The Australian Hydrological Geospatial Fabric (Geofabric V3) was downloaded for the North West Plateau and the Pilbara-Gascoyne regions from the Australian Bureau of Meteorology (BOM 2015). This data maps surface water networks, stream channel cartography, and catchments as vector data based on the 30 m resolution 2011 DEM. It includes small ephemeral streams as well as permanent water sources (i.e. major waterholes).

Bathymetric stream channels, however, are not mapped. To simulate where now-submerged, former stream channels may have been located, a hydrological analysis was conducted in ArcGIS on the 2021 seamless and hydrologically corrected 30 m terrain model, including identifying and filling sinks, flow direction, and flow accumulation analyses. Flow accumulation limits were set to visually match those from the Geofabric V3 and the results were smoothed to produce a polyline network that approximates potential permanent or seasonal submerged watercourses. The submerged stream channels were extracted and added to the Geofabric V3 data set to create the final seamless topographic/bathymetric hydrology data layer (Figure 19.1).

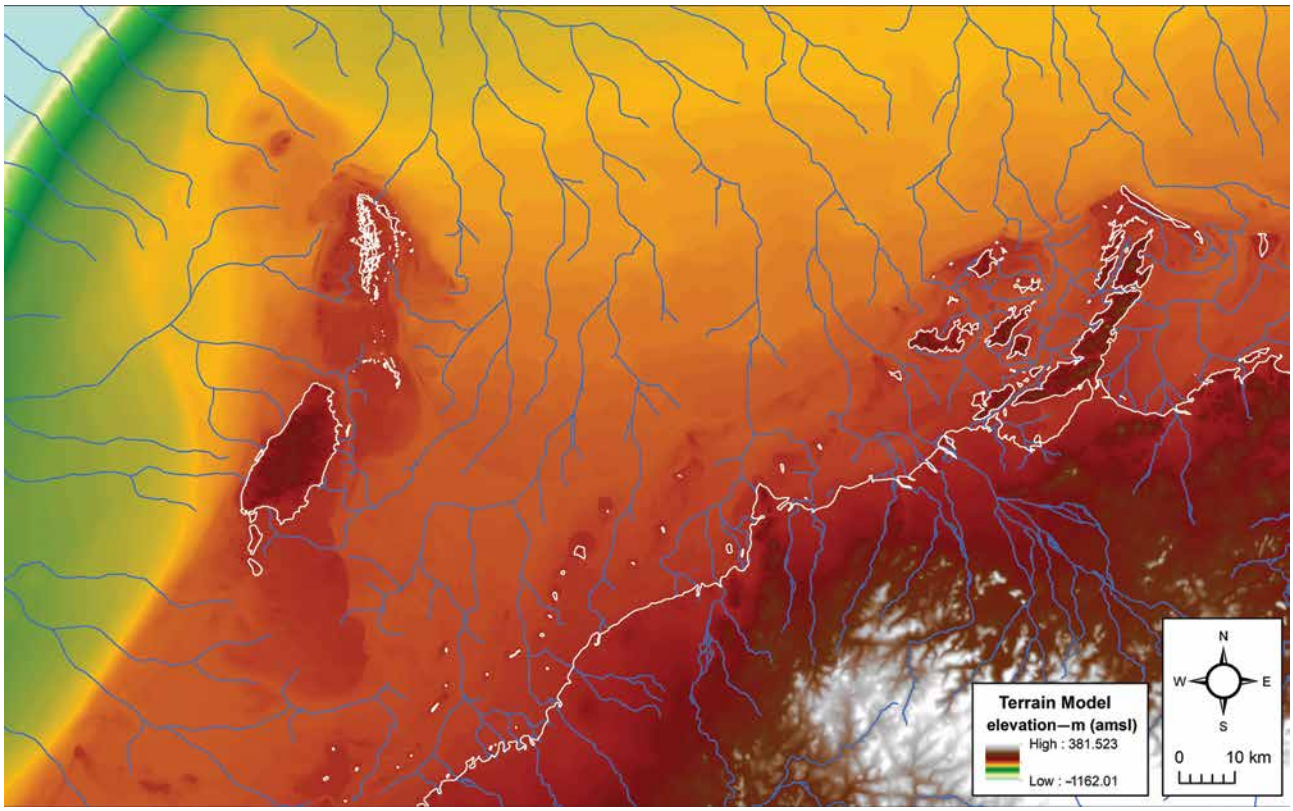

Figure 19.1. The seamless topography/bathymetry (from Lebrec et al. 2021a) and final hydrology model – modern coastline shown in white, major stream channels shown in blue.

This is by no means perfect data for the visualisation process but it is as accurate as can be achieved now. Again, this is a 'static' bathymetry, meaning that we recognise the very dramatic fluctuations of hydrodynamic forces on the 'true' bathymetry of the past: changes in fluvial sediment contributions to estuaries; wave diffraction effects on shoreline formation; inter-island current scouring; longshore and tidal beach erosion; storm surge and monsoonal effects; shoreline stabilisation by mangroves; seasonal and long-term tidal variability; and the erosion resistance of bedrock or secondary geological deposits. These hydrodynamic processes would affect not just the timing and shape of island formation, but the extent and availability of littoral zone resources throughout the entire sequence. By importing this data into a scenery generator, it is

possible to experiment with some of these effects to see how they *might* have changed the nature of islandisation around Murujuga.

Palaeoenvironmental Modelling

Spatially modelling palaeoclimatic data is far more complicated than working with terrain models and hydrology. While there are numerous errors to correct and ways to compensate for these, terrain data is generally systematically sampled directly, meaning there is physical terrain to be examined across the study area and that the data is inherently quantitative *across space*. Palaeoclimatic data is usually derived from indirect sources and very limited and unevenly distributed locations – through sea-floor or ice coring and geological or biological sampling (e.g. Collins et al. 2003, 2006; Magee and Miller 1998; Petit et al. 1999; van der Kaars and De Deckker 2002; van der Kaars et al., 2006; Vannieuwenhuyse et al. 2017; Ward et al. 2015; Woodroffe and Webster 2014). The data from those limited samples are projected across space based on simulated climatic patterns. These are compared with local physical conditions and contexts, with the result being a broadly probabilistic interpretation.

Changes in speleothem growth rates, pollen species abundance, palaeobotanical assemblages, sediment laminations, oxygen isotope ratios, tree-ring thickness, diversity in foraminifera and so on all contribute to a generalised *yet primarily qualitative* understanding of past climate (e.g. Bowler 1998; De Deckker et al. 2015, 2020; Denniston et al. 2013a, 2013b; Fitzsimmons et al. 2013; Griffiths et al. 2009; Hesse et al. 2004; Hiscock and Wallis 2005; Holdaway and Fanning 2014; Johnson et al. 1999; Miller et al. 2005; Reeves et al. 2013; Skippington et al. 2021; Veth et al. 2007, 2009, 2016b; Williams et al. 2013, 2015b; Wilson 2013; Wyrwoll and Miller 2001).

While an ice core, or speleothem, can give quantitative measurements for a specific location, ideas about how they apply across broader regions and landscapes are still highly interpretive. Our confidence in any particular representation of a palaeoclimatic model increases with a greater number of observations, a wider variety of measurements, more sampled locations, and closer in time to the modern day. Going further back in time is always problematic since there are fewer sources of data and they are usually more distant from the region of interest. It is very difficult to interpret how complex and diverse *local* palaeoclimates might have been, and it requires specifically local data.

Bearing this in mind, palaeoclimatologists have projected several different, largely quantitative data sets regarding sea-level changes over time, as well as models of global temperature change that can be applied locally *to some degree* (Claussen et al. 2003; Ganopolski and Rahmstorf 2001; Jouzel et al. 2007; Lambeck et al. 2014; Mahowald et al. 2006; Siddall et al. 2003; van der Kaars et al. 2006; Waelbroeck et al 2002; Yokoyama et al. 2001). There is also much more anecdotal or, at best, qualitative data available that indicates changes over time in terms of relative moisture level. Obviously, the further back in time one goes, the less accurate this data becomes. Yet by intersecting the observations from these sources and models, it is possible to generate a usable series of environmental projections for the experimental visualisations presented here. We reiterate that this approach is *experimental* and the visualisations reflect different hypotheses about past climates and effects: they are not *definitive* re-creations of what actually took place.

Sea levels

Following Ward et al. (2015), we employed the sea-level curves developed by Yokoyama et al. (2001), Waelbroeck et al. (2002), Siddall et al. (2003) and Lambeck et al. (2014) for this analysis. We extended the time frame back to 125 thousand years ago (kya) given this was the time that the Dampier Archipelago was last inundated. We also used the more locally specific sea-level curve from O'Leary et al. (2013). Since each source uses different data and comes to somewhat different conclusions, our use of these curves is divided into three different time slices:

- 0–35 kya – Lambeck et al. (2014) was used to calculate the range of modern sea level to about 15,000 years prior to the Last Glacial Maximum (LGM). We believe this source to be the most accurate for this time frame given the more intensive examination of the LGM maximum depths.
- 35–116 kya – Data from Yokoyama et al. (2001), Waelbroeck et al. (2002) and Siddall et al. (2003) were averaged for this period. Given conflicting sea-level modulations between these sources, we believed averaging them was sufficient for our visualisation purposes. This does not preclude rendering versions of the visualisations with any specific one of the sea-level curves, but that was not undertaken here.

- 116–125 kya – O'Leary et al. (2013) was the source for sea-level values during this time frame. Given this was the last high-stand, and there were specific questions regarding how the modern shoreline features relate to those of this previous high-stand, this more detailed model was chosen for visualisations of this period.

Each sea-level curve was formatted, scaled and digitised from high-resolution versions of the published figures with the X-axis representing the timeline and the Y-axis representing elevation above/below modern sea level (Figure 19.2). The Y-intercept was calculated for every 100-year period between 125 kya and today. This is not as accurate as finding the original data points and their probability ranges, and calculating a regression curve – but to generate this data would require an inordinate amount of processing. The 'shoreline' is a dynamic and fuzzy concept distinct from 'sea level' and must be taken into consideration with tidal range and local geomorphology (Larcombe et al. 2018). The crucial point with respect to these visualisations is how the shoreline dynamics integrate with landscape change on multiple scales, and not an adherence to one specific model for absolute sea-level values.

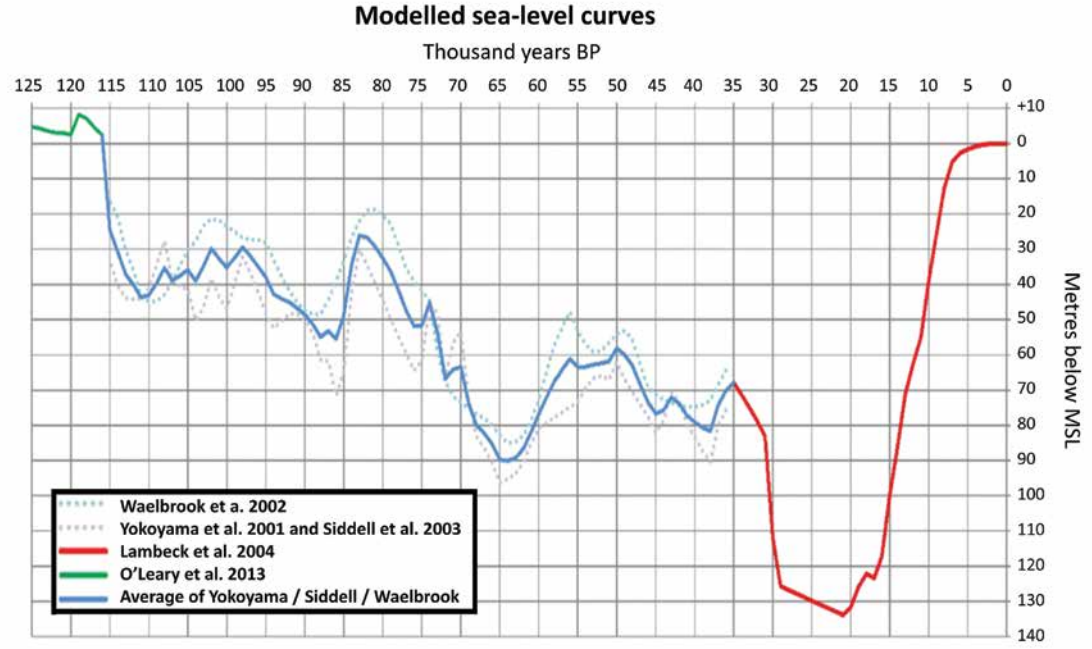

Figure 19.2. Sea levels used in the Terragen visualisations.

Temperature and moisture

Whereas local physical characteristics can be used in conjunction with global sea-level models to help clarify where the 'shoreline' was, there is far less local data to validate global temperature and moisture models. The most widely used models for deep time global temperature change come from the Vostok ice cores from central Antarctica (Petit et al. 1999; Jouzel et al. 2007). Climatic modelling and simulation based on those values, along with other data sources, expand upon climate conditions worldwide (e.g. Claussen et al. 2003; Ganopolski and Rahmstorf 2001; Mahowald et al. 2006; Van Meerbeeck et al. 2009).

Although these sources provide specific quantitative data for atmospheric gases and other parameters through deep time, their complexity over the span of our visualisations makes it difficult to comprehend the regional climate and local micro-climates. For that we turned to more qualitative information, such as radiometrically dated geomorphological contexts; proportional plant species representations in pollen, floral and faunal assemblages recovered from archaeological sites; or inferences from coral reef growth, sedimentary cores, stalagmites and so on (e.g. Bowler 1998; Collins et al. 2003, 2006; De Deckker et al. 2015; Denniston et al. 2013a; Griffiths et al. 2009; Magee and Miller 1998; Miller et al. 2005; Skippington et al. 2021; van der Kaars and De Deckker 2002; van der Kaars et al. 2006; Vannieuwenhuyse et al. 2017; Veth et al. 2009, 2016a; Ward et al. 2015; Woodroffe and Webster 2014; Wyrwoll and Miller 2001). Synthetic and comprehensive discussions

were also used to develop relative measures which could be employed within the ArcGIS models and Terragen visualisations (e.g. De Deckker et al. 2020; Denniston et al. 2013b; Fitsimmons et al. 2013; Hesse et al. 2004; Hiscock and Wallis 2005; Holdaway and Fanning 2014; Johnson et al. 1999; Reeves et al. 2013; Veth et al. 2007, 2016b; Williams et al. 2013, 2015; Wilson 2013).

Compiling data from these various sources produces some categories of climatic variables, geomorphic conditions or vegetative communities that affect how we develop the 3D visualisations in Terragen. It is also clear from this analysis that we do not know exactly how the temperature changes relate to, or differ from, specific moisture levels. But we were most concerned about changes in overall moisture and temperature combined, increases/decreases in seasonal monsoons, the effects on coastal erosion, reef-building, the growth of mangroves, stabilisation of the littoral zone, changes in fluvial permanence, the availability of fresh water, and the expanding or contracting of interior dune fields. Some of the relative patterns employed for modelling major climatic indicators over the long term are illustrated (see Figure 19.3) as a shaded function of intensity (in reef or dune building) or difference from the current average (for combined temperature/moisture) over the entire time span.

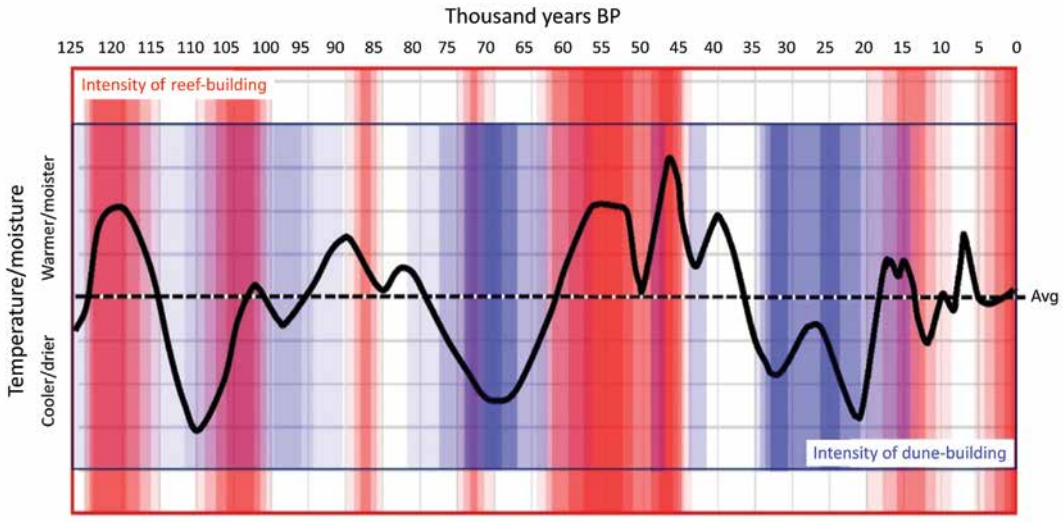

Figure 19.3. Relative climatic indicators over time used in the Terragen visualisations. The black line is a composite of temperature and moisture; red indicates intensity of reef-building and blue indicates intensity of dune-building.

From the compiled data sources, we modelled periods with higher-than-average general moisture levels between 123–117 kya, 92–88 kya, 58–53 kya, 48–45 kya, 42–39 kya, 18–15 kya and 8–6 kya. Drier than average periods were modelled between 112–108 kya, 77–62 kya, 33–20 kya and 13–9 kya (see Figure 19.3). Changes in temperature and monsoons generally followed the same patterns, with increased monsoonal activity and fluvial permanence during warmer periods but with a lot of local variability simulated by the visual fractalisation. Relatively dramatic changes occur to sea level during spans between 116–111 kya, 86–83 kya, 74–64 kya, 35–26 kya and 18–6 kya (see Figure 19.2). Most other time frames indicate smaller fluctuations or moderately stable shorelines and/or climatic conditions, with very stable periods occurring only between 123–119 kya, 110–100 kya, 57–51 kya and 5–0 kya.

We have not included the dramatic increases in temperature attributable to climate change in the modern era. The '0' date in the chart correlates to a time around 150+ years ago (c. 1870) that pre-dates any historic modifications of the Murujuga landscape, such as roads or settlements. These were not digitised as part of the terrain model, and any climatic changes after 1870 were also not included.

Some of the data sources are contradictory with regard to the LGM and relative moisture levels. More information is needed to develop accurate models of regional or micro-climatic variability. In our simulations, micro-climatic variability is inserted only via fractal patterning and is not extracted from physical data, because the local data does not exist or it is highly fragmented both temporally and spatially. But overall, these trends give us something to work with in establishing a visual frame of reference for 3D landscape modelling.

3D Landscape Modelling

Terragen 4.6.11 is a 3D modelling software package known as a 'scenery generator' which uses a connected set of modules (terrain, water, lighting, atmosphere, shaders, objects and cameras) to render high-resolution still images and animations taken from specified locations. It is widely used in the film industry to generate both realistic and otherworldly landscape imagery as digital backdrops for green-screened areas. Terragen (in various releases) has been used in recent films *Thor: Ragnarök* and *Star Wars: The Last Jedi*, and on television in *Game of Thrones*, among many others.

Terragen software is a tool for artistic rendering. However, it is designed to simulate real-world physical processes as the basis for such interpretations. The objective of its use here is to render photorealistic imagery that conforms to our visual and physical expectations – not merely as an artistic interpretation but based on quantitative and qualitative data. Existing and modified terrain data can be imported into Terragen as a natural extension of the GIS modelling environment, allowing us to illustrate photorealistic textures and to animate long-term geological or environmental processes (such as sea-level rise and fall, erosion and changing ecosystems) on data-derived surfaces.

Terrain

Terragen can generate a random elevation data set or one using various forms of fractalisation to create visually realistic landforms. It can also import real terrain data that has been processed in ArcGIS. For this analysis, the digital terrain models (the initial corrected 2015–2017 version and the 2021 version) were exported as GeoTiff files and imported into Terragen as the base terrain layer in each visualisation. These data sets are ~243 km east–west by ~153 km north–south in overall size and have a measured elevation value spaced every 30 m at a minimum. The terrain layer is fixed to a virtual globe that simulates the dimensions and curvature of Earth.

Unlike a GIS, or a conventional 3D object-editable environment, Terragen interpolates between measured elevation values by adding randomised height variation calculated using fractal geometry. In this case, we applied only a small amount of fractalisation (half of the default amount) with a limited variation that cannot exceed 1.5 x the difference between any two measured points. Fractal detail adds roughness to the terrain that approximates a photorealistic rendering and is an important aspect of rendering most other surfaces and textures in Terragen as well, such as geologic layering, distributions of plant communities, and reflections on water surfaces.

Daniil Kamperov's (2020) Classic Erosion plugin for Terragen provides simulated erosion effects, and was used as a permanent, but static, minor displacement layer. It did not substantially alter the initial elevations but provided some realistic definition that worked in tandem with the fractal effects and was consistent with the hydrological modelling.

Water

The water module is where the parameters are defined for the placement, extent and elevation of the ocean in the 3D visualisation. Here, we created an ocean surface that matched the extent and size of the terrain layer. Since it is also attached to the planetary object (like the terrain layer), water accurately follows the curvature of the Earth. Thus, views of objects or land on the horizon are represented the same way, and at the same scale, as they would be in real life.

The ocean surface parameters can include transparency, wave scale, roughness, decay tint, decay distance, volume density and volume colour. For this analysis we used primarily default settings but kept a smooth surface, and altered the decay tint to slightly more greenish, or turquoise, hues that better represent a tropical water column. Transparency and depth of decay becomes virtually opaque at a depth of 10 m below the modelled sea level to depict a comparable littoral zone of approximately the first 10 m of depth for all animation frames.

To generate an animation, Terragen renders a series of frames that are then exported to a video editing platform to be sequenced and edited as the final animations. For this analysis, we defined 1,250 frames, each of which was designated as a 100-year increment in the analysis. The combined sea-level value (from the curve illustrated in Figure 19.2) was calculated for every 1,000 years and set as the elevation for the ocean layer at every tenth frame, with frame #1 representing 125 kya and #1250 representing the c. 1870 shoreline. Ocean levels for the nine frames, in-between each set elevation value, were mathematically interpolated by Terragen along a smooth curve.

Lighting

Modifying the parameters of sunlight and the effects of direct and atmospheric light on the terrain and water surfaces is done in the 'lighting' module. Many animations use the movement of the sun across the sky to change the ground effects, shadows, reflections and ambient illumination of the landscape. As we spanned 125,000 years of landscape change, we kept the exact same lighting and atmospheric parameters for all animation frames. But for ground-level visualisations, we chose different lighting and atmospheric parameters to help provide realism, illuminate plant communities, and sometimes impart a sense of visual depth to the scene.

Terragen allows for control of sun objects by heading, elevation, colour and strength. For the animations and still images taken from the low earth orbit and oblique aerial perspectives, the heading of the sun was set to 300 degrees N, at an elevation of 12 degrees above the horizon, or the equivalent to around 6:30 pm on 5 June near the location of Karratha. This was checked using NOAA's (2022) solar position calculator. The heading and elevation (in the animations) were chosen to provide horizontal raking light across the landscape that would help make low hills and terrain features stand out at long distance. The colour of the light is slightly more golden and set at a slightly higher than default strength to enhance this as well.

Atmosphere

The 'atmosphere' module allows the control of parameters affecting the landscape illumination: suspended particulate matter (haze), clouds and reflected light. Here we also kept things equal throughout the entire time span for the long-sequence animations. Default parameters were used for most of the visualisations, with a slight amount of haze and the addition of a small amount of red-sky additive to simulate the effects of the low angle of the sun. A very high layer of light global cloud cover was inserted to soften the shadows cast on the ground and/or the surface of the ocean. For individual ground-level views, separate incidences of different cloud patterns were inserted to create realistic backdrops when the horizon was visible to the camera. Some low earth orbit, or aerial oblique, images or animations that do not include horizon views may also contain cloud layers, though they might only be visible as shadows on the ground.

Shaders

The use of shaders is the primary means of creating realism in the modelled landscape from the low earth orbit and aerial perspectives. These are individual layers, ordered stratigraphically, that can simulate bedrock, sediments, vegetation or other terrain disturbances. As shaders were created, they were compared to visualisations from Google Earth from the same, or similar, perspectives. For this analysis, 18 primary shaders were created in three major categories:

- *Geology* – All of the hard rock geology layers are static (do not change with animation) and are organised to lie stratigraphically beneath the surface sedimentary and vegetation layers. They include the basal bedrock layer, light-coloured surface rocks, dark-coloured surface rocks, and two distinctive bedrock layers for Murujuga and the Pilbara uplands. Fractal patterns are used to distribute a mixture of both light and dark surface rocks across the terrain, while slope, elevation and manually painted geological limits and/or aerial imagery help the gabbro and granophyres of Murujuga and the Pilbara Craton formations stand out through the overlying vegetation.
- *Surface sediments* – Several surface shaders were situated on top of the geology layers to simulate dynamic geological processes that would be visible from multiple perspectives. This was predominantly related to the tidal and littoral zones, but also to patterns of dune formation. The shaders used were littoral zone marine sands, tidal flats, beach sands, and interior sand dunes. Tidal flats were simulated where broad expanses of very flat tidal areas occurred with finer silts, or mud, and they diffuse gradually into the marine sands beneath sea level.
- *Vegetation* – The vegetation layers overlie the geology and the sediments and are designed to represent distinctive communities of plants. They include spinifex and other bunch grasses, mixed shrubs and understorey, acacia-dominant shrublands, lowland eucalypt forest, semi-open dry woodlands, coastal tropical forest, riparian woodlands, underwater vegetation, and mangroves. Changes in the visual representation

of these communities were tied to changes in sea level directly, limited by a GIS-derived falloff from the hydrological stream channels, and increases or decreases in both temperature and moisture. Sensitivity to moisture level was controlled not just by coverage, but also by increasing or decreasing the amount and/or scale of fractalisation. Colouration of individual shaders was derived by comparing to aerial imagery from the study region and adjacent areas.

Objects

Whereas shaders are the primary means of adding visual realism from low earth orbit or aerial perspectives, ground-level views require more complex 3D models. Plant models from Xfrog and Silva3D were used as well as other shareware 3D objects collected from various sources and internal objects native to Terragen. The plants and other objects are realistic, highly detailed, fully textured meshes designed for use by CGI specialists, artists and animators using a wide range of 3D modelling applications.

The archaeological and palaeobotanical records discussed earlier were used to select the plant object populations depicted for each time period. However, the manner in which they are arranged is based primarily on comparison with descriptions and images in Mitchell and Wilcox (1994), Petheram and Kok (2003), Moore (2005), van Osterzee (2009), Wilson (2013) and the FloraBase (2022) by the WA Department of Biodiversity, Conservation and Attractions. Any species which was not available as a 3D plant model was substituted with a similar available model, which then was edited in Terragen or 3ds Max (Autodesk 2017–2022) to reflect appropriate differences in colouration, size or shape. Unless otherwise noted, all 3D objects were acquired online through shareware non-attribution sources.

Camera locations

Each Terragen frame is rendered from the location of a camera situated in the virtual environment. Cameras are designated as either fixed locations or are calculated to lie along a path or curve, and set to move a specified distance between frames. Cameras have settings for aperture, focal depth, exposure and so on, along with orientation in three dimensions. For the visualisations presented here, a wide range of camera locations were experimented with and situated in the landscape at various locations. These fall into three general classes:

- *Low earth orbit* – This is a single camera set very high in altitude (about 200 km) and looking down at a 90-degree angle to encompass the entire terrain model. This is the preferred perspective for viewing long-term sequences.
- *Oblique aerial* – Several cameras were situated at varying heights and looking obliquely at specific target areas. They tend to range from 10 to 20 km in elevation (above modern sea level) for higher altitude oblique views, and as low as 100–1,000 m for lower altitude obliques. Oblique cameras were chosen specifically to illustrate landscapes or temporal sequences.
- *Ground level* – Multiple cameras are situated at ground level or close to it across the study area, but their specific contexts and settings change depending on the nature of the time frame being illustrated. The examples presented here are intended to illustrate the changing landscapes from a single point of view at significant moments in the past. Ground-level cameras are typically positioned between 1.5 and 20 m above the ground surface and look primarily nearly level towards the horizon or a specific target of interest.

Dynamic terrain modifications

As some of the outcomes from the 3D modelling are animations simulating lengthy periods of time, we know that dynamic geological and hydrological processes will alter the appearance of that terrain to some degree and at various times. Terragen gives us the ability to apply modifications to the base terrain model in each frame prior to generating the overlying surfaces. This is conducted using 'displacement' shaders attached to the terrain module which will increase or decrease, by a specified amount and in a systematic way, the positional value of any location in three dimensions. The benefit of displacement shaders is that they can simulate long-term geological or erosional changes to the GIS-generated terrain.

We experimented with some of these effects for this project. They include one which simulates the long-term sequence of shoreline erosion on bedrock features, and several others related to the addition or removal

of sediments in the littoral zone simulating fluvial, wave and tidal effects. First, we considered that since the last sea-level high-stand was at 125 kya, it was very likely that some of the remnant shoreline cuts we can still see today (in areas above modern sea level) are surfaces from previously more extensive geological formations and beach rock that have been eroded by persistent wave action. A pre-erosion terrain was simulated by creating a displacement shader that altered the terrain surface by a maximum of +3 m based on slope and only within the moving littoral zone but dropping off over the length of the animation. Where the terrain was more level, this effect was enacted less and was instead replaced by sedimentary depositional or erosional effects.

The second dynamic hydrological effect occurs on the sedimentary layers rather than bedrock. This is the effect of increased or decreased sediment load entering the littoral zone through fluvial action. Based on a simplification of large regional processes (described in Larcombe et al. 2018), we experimented with the idea that a warmer and wetter climate would entail longer duration and output flow from streams and rivers. This output would increase the suspended sediment contribution to the littoral zone and ultimately lead to increased deposition in certain near-shore areas. In contrast, a cooler and drier climate would decrease the corresponding fluvial sediment load, and erosion of sediments near those same areas would increase (de Deckker et al. 2015). This was simulated with an inverted exponential cost-distance evaluation from the projected stream channels used as a mask to displace as much as ±4 m of sediment in submerged near-channel areas and is based on terrain slope and climatic conditions for each frame of the animation. Warmer/wetter periods increase sediment load, while cooler/drier periods decrease it.

A third dynamic displacement shader was created to simulate the effects of wave diffraction around the edges of islands and other shoreline formations. To model this, we created two wave diffraction displacement shaders. The first is tied to the lateral edges and back sides of island formations as simulated by the static bathymetry at 10 kya. It gradually increases sediment deposits in these locations to a maximum of +5 m and then gradually diminishes beginning around 6.5 kya. It is overlapped with and slowly replaced by the second displacement which targets the lateral edges and back sides of island formations as simulated by the static bathymetry beginning around 7 kya. It increases to a maximum of +5 m of added sediments by 3.5 kya and then gradually diminishes until it disappears by 0 kya. This overlapping of intensity and areas of application simulates only the last 10,000 years of islandisation and only during the initial modelling phase (2015–2018). This displacement was not added for the most recent modelling phase (2021–2022), which used the more recently developed terrain model.

Visualisations

Terragen visualisations are rendered both as animations and as still images. Animations are initially rendered as a sequence of frames – either the entire 1,250 frames or portions representing specific time periods. As animation frames, the output resolution is set at 3800 by 2375 pixels, and each frame takes between five to eight minutes to render, depending on the complexity of shaders in the view. Each set of 1,250 frames then takes between 104 and 167 hours of rendering time on a Windows 10, AMD Ryzen 9 5950X 16-Core CPU, 3.41 GHz, x64-based desktop with 64GB of RAM. Animation sequences were set to render overnight or across several days. Ground-level images were rendered at higher resolutions, up to 6400 by 2400 pixels, and each one would take as long as several hours to complete.

One full-sequence animation was generated with the camera situated at low earth orbit (Whitley 2022). This sequence of renders starts at 125 kya and illustrates the general trends in shoreline transitions from a long-distance perspective. The generalised locations of relevant archaeological sites are included to give reference points to known human occupation. They appear at the frame matching their earliest recorded radiocarbon or OSL dates.

125 kya to 85 kya - Last interglacial period

Several interesting observations can be made from the different visualisations. While there is scant evidence to suggest human occupation of Australia occurred as early as 125 kya (see McNiven et al. 2019), this last high-stand further etched the current archipelago's shoreline. Beach rock dates to this period at several key locations (Benjamin et al. 2020). A low earth orbit visualisation at c. 118.5 kya, focused on Murujuga, illustrates the maximum high-stand (Figure 19.4) on the simulated pre-eroded surface.

Figure 19.4. Low earth orbit visualisation of Dampier Island (Burrup Peninsula) c. 118,500 years ago.

This visualisation sees Dampier Island (the modern Burrup Peninsula) as fully detached from the mainland. However, as modern topography and bathymetry are conditioned by prior processes, we cannot be sure of the palaeo landforms at that time. While we can simulate past ecosystems atop modern terrain, or modify these with hydrodynamic effects, we need to remember that any attempt at projecting past human colonisation or settlement should consider the underlying nature of this terrain and its relationship to such processes. For that, we still lack much detail.

The climate for the period 125–115 kya was warmer and wetter, coinciding with a period of relative sea-level stability (Fitzsimmons et al. 2013; O'Leary et al. 2013). This suggests that reefs were building up, shellfish beds and mangrove habitats were likely expanding, and shoreline movement was minimal. But then sea level dropped dramatically for the next 5,000 years, as did temperature and moisture levels. Shellfish beds and reefs would have been left high and dry as shorelines rapidly retreated.

Between 110 kya and 97 kya, sea level stabilised and climatic conditions returned close to modern levels. Reef-building probably intensified again during this early phase, tapering off as sea level began falling again between 97 kya and 85 kya. The very flat terrain north-west of Murujuga indicates that even slight changes in sea level would translate into broad shoreline movement. Tidal- and fluvial-dominated scenarios indicate elongated estuaries and stream channels separated by broad mud flats and tidal lagoons during this period. But where offshore terrain is much steeper,

the hydrodynamics suggest wave-dominated, much narrower and more stable shorelines.

85 kya to 60 kya – Early potential colonisation

Sea level rose rapidly from 85 kya, before starting a long slow decline again between 82 kya and 65 kya. This period corresponds to the early maximum date currently accepted for human occupation of Australia (Clarkson et al. 2017). The lowlands fed by the Maitland, Fortescue and Robe rivers were expansive and comprised a patchwork of grasslands, scrub, coastal forest and riverine woodland. As sea level fell, various estuaries and islands would have been available for human occupation on this colonisation shoreline (e.g. the large embayment that emerged around 75 kya (Figure 19.5).

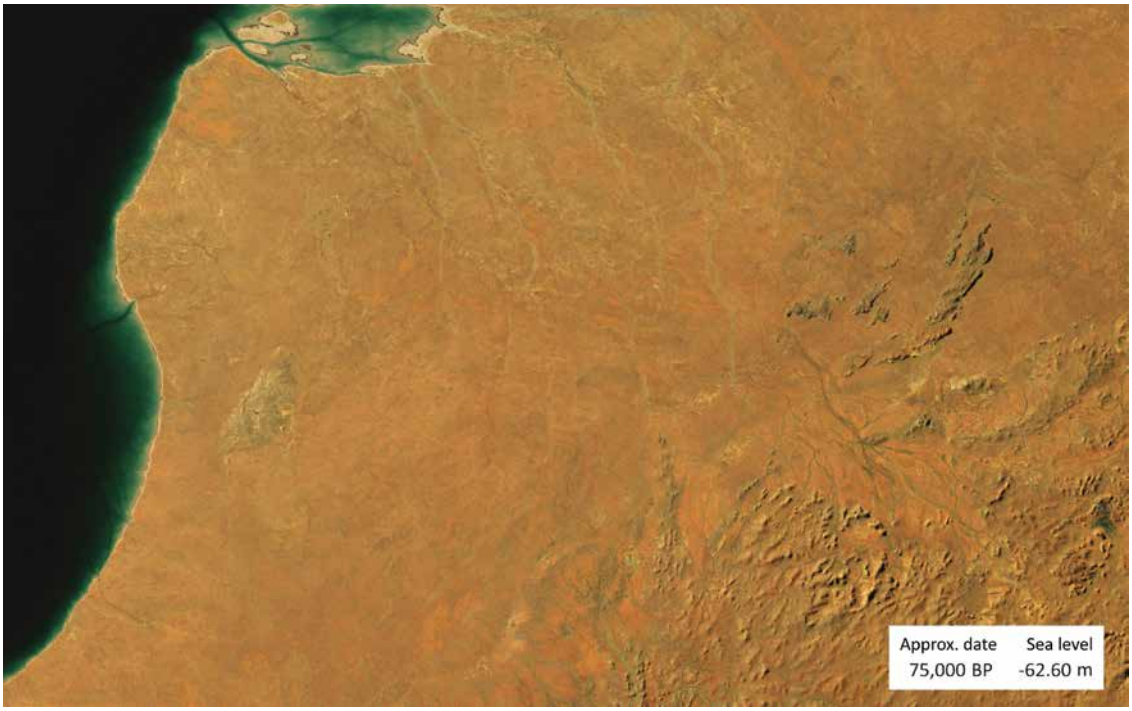

Figure 19.5. Low earth orbit visualisation c.75,000 years ago.

60 kya to 35 kya – Relatively stable conditions

Between 60 kya and 35 kya, sea level remained fairly constant. Reef-building increased while mangroves and shellfish beds also likely re-established. An increasingly warmer and wetter climate brought the onset of a more regular monsoon. By 50 kya, Boodie Cave (on Barrow Island) had human occupation (Veth et al. 2017) and lowland eucalypt forest and wetland habitats expanded across the broad coastal plain into the interior.

This lowland eucalypt woodland extended about 40 km to within 4 km of the modern-day Rosemary Island (Figure 19.6). This viewpoint faces north-east with the Rosemary Island interior being in the background.

Dominant trees are river gum (*Eucalyptus camuldulensis*), snappy gum (*E. leucopholia*) and ghost gum (*Corymbia bella*), while the dense understorey comprises a mixture of grasses, including bunch speargrass (*Heteropogon contortus*) and sorghums (*Sorghum* spp.). The species used in these visualisations are examples of plant communities from modern environments in similar contexts to the period being depicted (i.e. it does not definitively identify dominant species at the time).

Near the southern end of the Burrup Peninsula at 50 kya, the visualisation looks south-east from a ridgeline of typical Murujuga rock formations (Figure 19.7). The relatively warmer and wetter environment supported a semi-open woodland of mixed eucalypts and figs with denser stands of river gum, with ghost gums in the wetter areas in the distance. The ephemeral drainages leading up the slopes are punctuated with smooth-barked coolibah (*Eucalyptus victrix*) and cycads (*Cycas* spp.). In the right foreground are several small rock figs (*Ficus platypoda*), and on the left is a northern quoll (*Dasyurus hallucatus*).

(Above) Figure 19.6. Ground-level visualisation offshore from modern Rosemary Island c. 50,000 years ago.

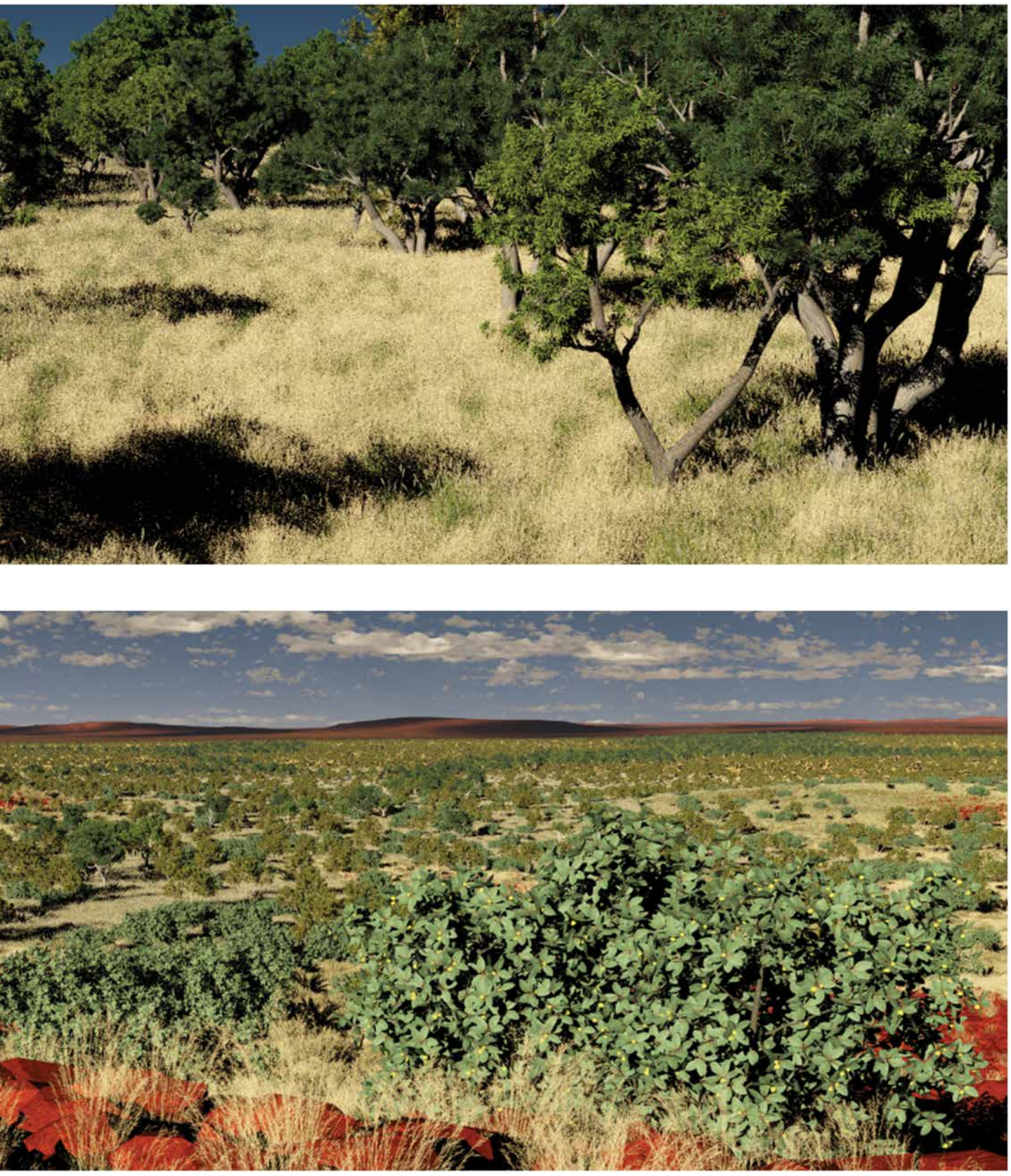

(Below) Figure 19.7. Ground-level visualisation of the ridgeline on Murujuga c. 50,000 years ago.

(Above) Figure 19.9. Ground-level visualisation offshore from modern Rosemary Island c. 20,000 years ago.

(Below) Figure 19.10. Ground-level visualisation of ridgeline on Murujuga c. 20,000 years ago.

35 kya to 17 kya – Cooling and drying climate

Around 35 kya, sea-level shorelines shifted horizontally along the steeper edge of the continental shelf. Despite a narrower band of movement, the littoral zones were probably not shallow enough along this coastline to promote reef-building, establishment of mangroves or extensive shellfish beds. Instead, it was probably a wave-dominated coastline, with narrow sandy beaches, backed by steep rocky hills and scrub- or dune-covered terraces.

During the Last Glacial Maximum, peaking at 21 kya, the climate was dry and sea level reached its minimum, around –134 m. Despite this, occupation is recorded at both Noala and Murujuga rockshelters (Figure 19.8). The expansive lowland and coastal acacia woodland and/or riverine eucalyptus forest would have been replaced with scrublands or grasses. The more well-watered vegetated areas along low-lying stream channels may still have contained isolated seasonal waterholes and some sparse coastal forest fed by offshore moisture patterns.

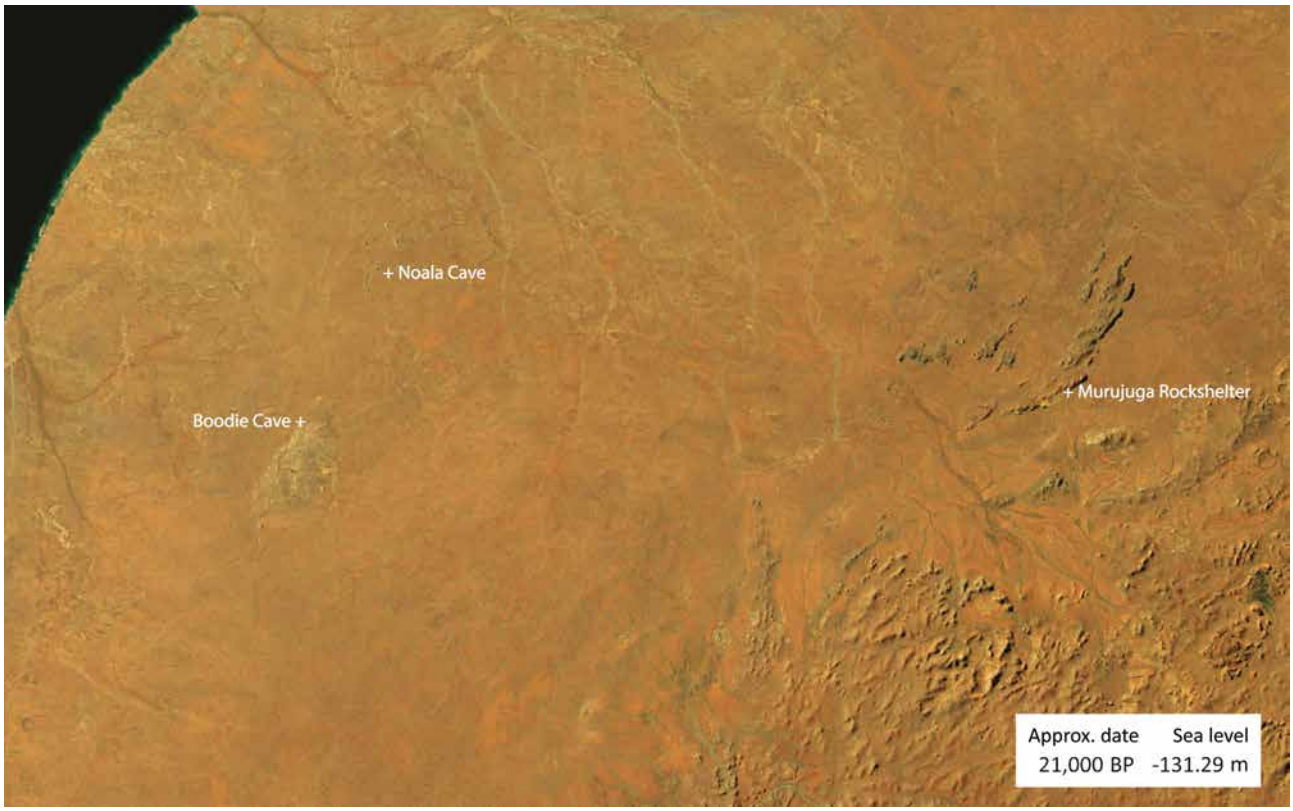

Figure 19.8. Low earth orbit visualisation of the North West Shelf c. 21,000 years ago.

At 20 kya, the ground-level visualisation shows Rosemary Island, which is still over 120 km from the shoreline (Figure 19.9). The plain is dominated by limestone spinifex (*Triodia wiseana*) with a few other hardy tussock grasses, punctuated by scattered blue mallees (*Eucalyptus gamophylla*). Seen from the Murujuga heights (Figure 19.10), this landscape is much drier and sparsely vegetated. Limestone spinifex (*Triodia wiseana*) dominates with scattered blue mallees (*Eucalyptus gamophylla*), Kanji bushes (*Acacia pyrifolia*) and mulgas. In the distance are occasional desert oaks (*Allocasuarina* spp.).

17 kya to 10 kya – Rapid sea-level rise

The sea level remained near LGM level until after 15 kya, when there was a rapid increase in sea-level rise corresponding to an increase in monsoonal activity and a warming climate.

With a rapidly rising sea level and relatively flat terrain and warming conditions, the near-shore conditions would have been dominated by massive mud flats, displaced sediments, heavily eroding shorelines and devegetated zones. Maritime economies would have been destabilised with littoral zone species, shellfish, reefs and mangroves being generally sparse across the study area. Steeper sloped, inter-estuarine areas of less erodible bedrock may have fared better, as they would be more likely to form peninsular bridges to more open, often less turbid, water.

Around 10 kya, a broad swathe of the northern study area has opened up into a wide bay, as the former river plains are inundated (Figure 19.11). Narrower, elongated estuaries begin forming as sea-level rise starts to slow and more downcutting begins. This is also the point at which regional islandisation begins to occur, with the outer Montebellos being cut off. The Murujuga uplands are now situated pretty close to the encroaching shoreline.

Figure 19.11. Low earth orbit visualisation of the North West Shelf c. 10,000 years ago.

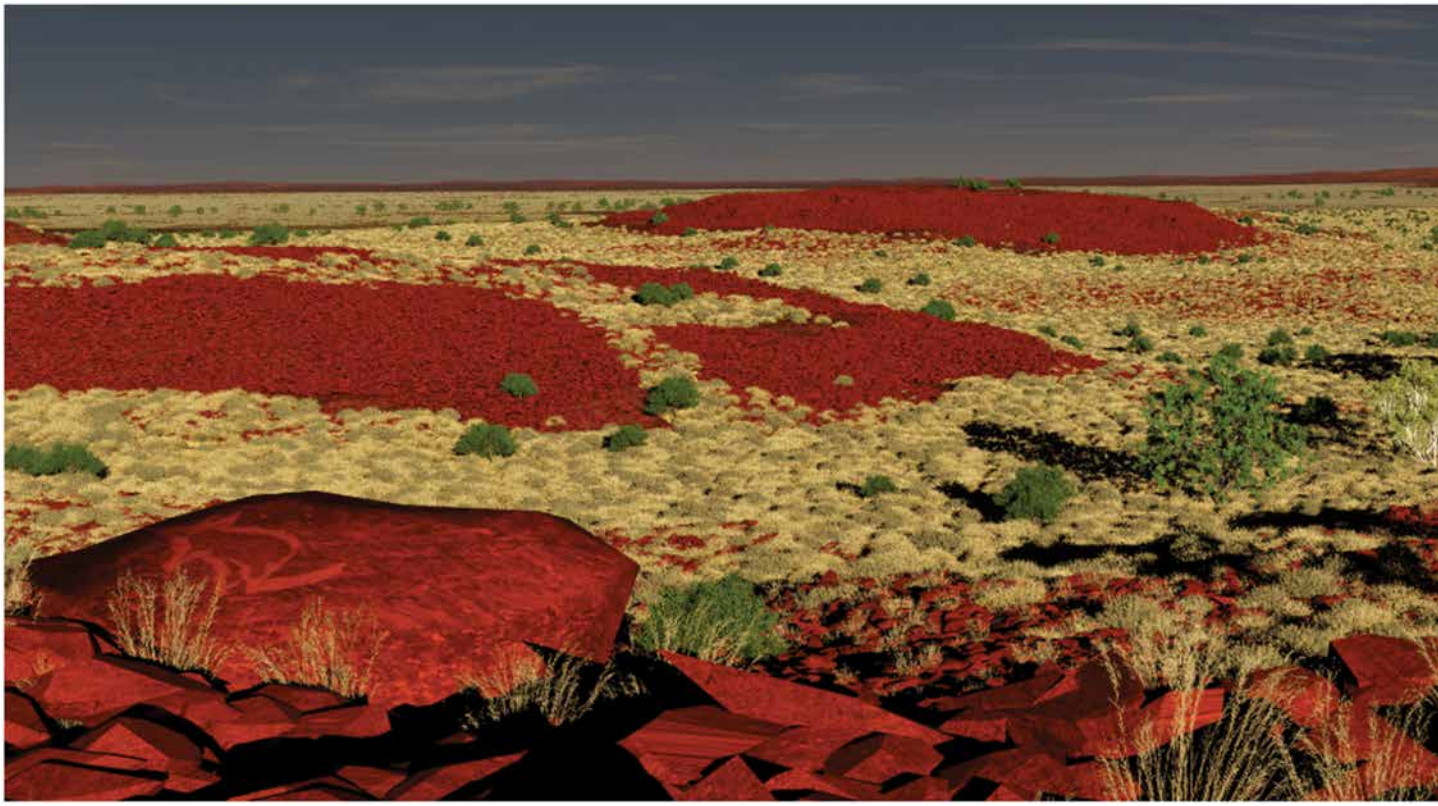

(Above) Figure 19.13. Ground-level visualisation offshore from modern Rosemary Island c. 8,000 years ago.

(Below) Figure 19.14. Ground-level visualisation of the ridgeline on Murujuga c. 8,000 years ago.

10 kya to 0 kya – Intensive islandisation

After 10 kya, shorelines begin to approach their modern configuration. At 8 kya Rosemary and Malus islands were joined, as were the two Lewis islands. Enderby was an island but much larger than its current extent and joined by a land bridge to Goodwin Island. All the inner islands, Burrup and north to Legendre, are still part of a peninsula attached to the mainland (Figure 19.12). As sea-level rise decreased, we would expect that shorelines were eroding less, littoral zones were less turbid, and maritime resources would have become much more abundant. Reef-building would have increased during this period, and tidal species would have been able to re-establish themselves.

Figure 19.12. Low earth orbit visualisation of the North West Shelf c. 8,000 years ago.

The c. 8 kya ground-level visualisation (Figure 19.13) shows the shoreline about 2 km to the north-west of Rosemary Island. The most abundant plants are bunch-grasses, along with various mulgas (*Acacia* spp.) and Kanji bushes (*Acacia pyrifolia*). The nearest estuary is around 2 km to the south, as the strait between Rosemary and Enderby islands evolves. A distant line of eucalypts in the image marks a wetter area parallel to the uplands, near the modern Rosemary shoreline. As the shoreline was rapidly approaching from the north-west, extensive sand dunes (created during earlier, drier periods) were being pushed by prevailing winds to the south-east and eventually subsumed by inundation or eroded by aeolian processes. These sediments eventually covered the rocky terrain and became part of the littoral zone seen in the next two ground-level visualisations from this location.

Inland along the Murujuga ridgeline (Figure 19.14), the density of spinifex, tufted grasses and mulgas has increased dramatically. The coolibah have recolonised the seasonal washes, and larger eucalypts are becoming more numerous along the more permanent waterholes in the distance. The view is still of a vast, mostly treeless plain with the shoreline located some 20 km distant. In the lower foreground a line of desert honey myrtle (*Melaleuca glomerata*) occupies the sloping ephemeral wash. A recently created rock wallaby petroglyph can be seen on the large boulder to the left.

By 4 kya, the shorelines are very close to their modern configuration (Figure 19.15). The archipelago re-establishes itself rather rapidly, readapting to previous shorelines notched by the last interglacial high sea stand. Each modern named island was evaluated for its shallowest connection to the mainland or next adjacent island, and approximate separation and submergence dates were calculated, with time scale being a branching tree diagram (Figure 19.16).

Figure 19.15. Low earth orbit visualisation of the North West Shelf c. 4,000 years ago.

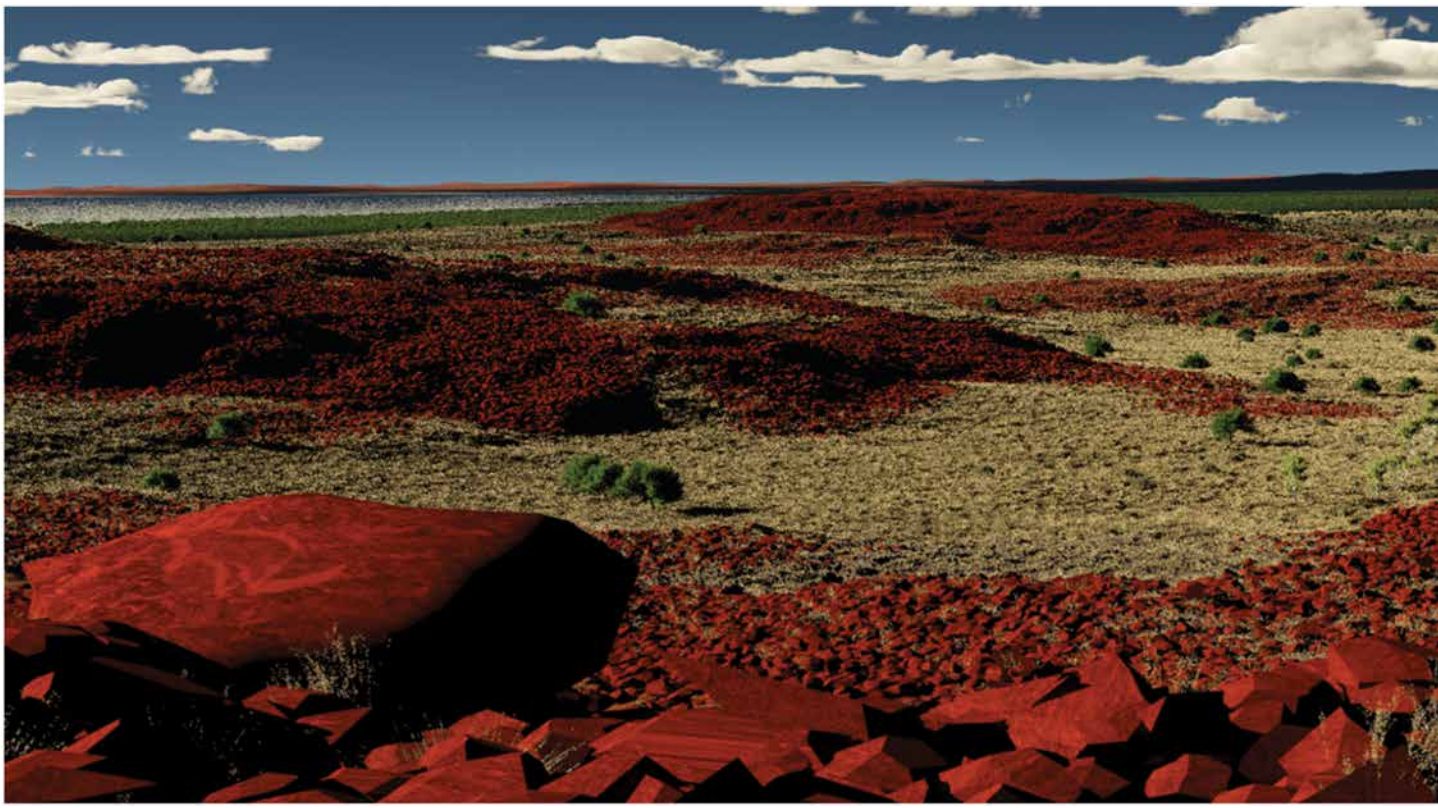

(Above) Figure 19.17. Ground-level visualisation offshore from modern Rosemary Island c. 4,000 years ago.

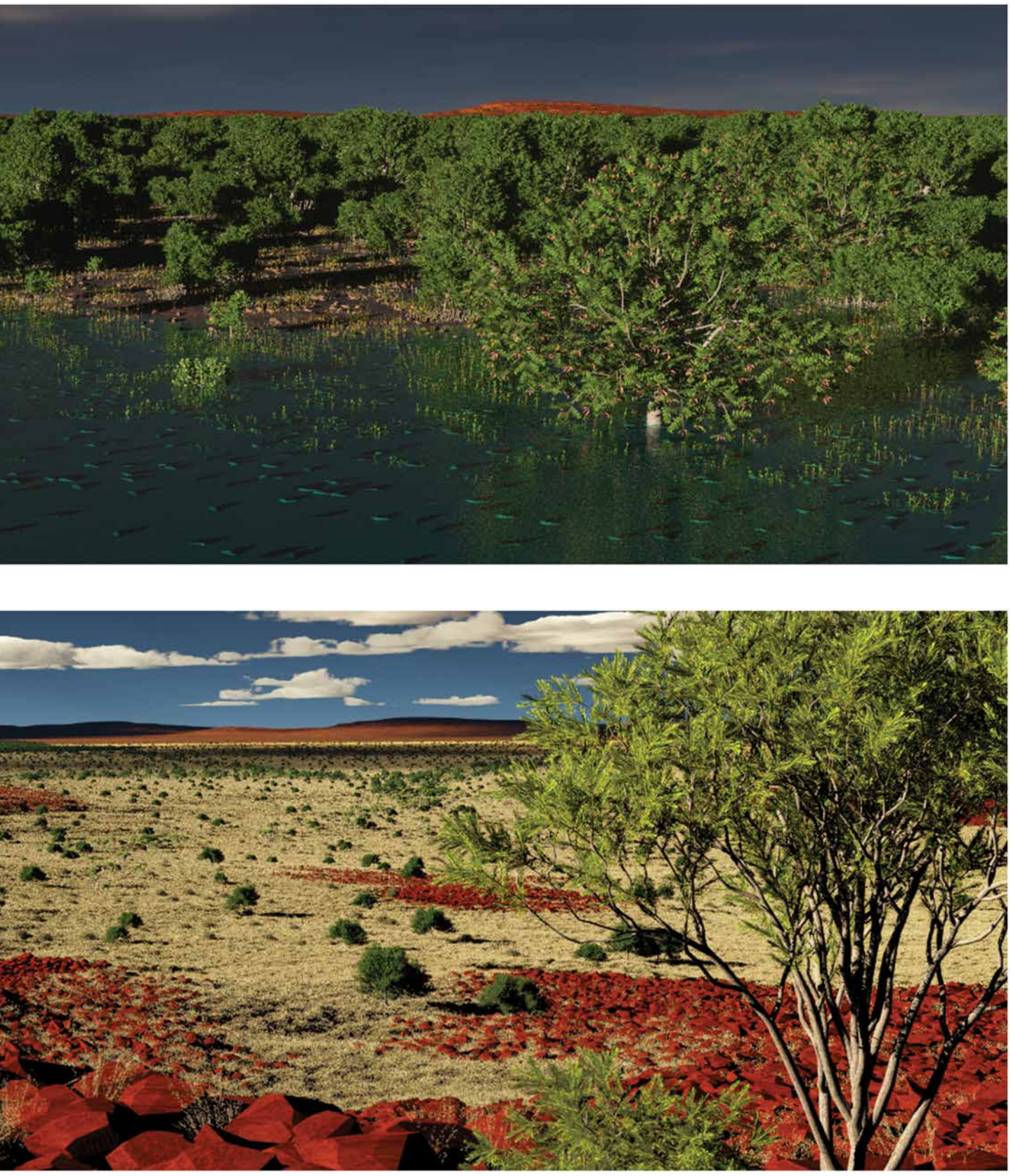

(Below) Figure 19.18. Ground-level visualisation of th eridgeline on Murujuga c. 4,000 years ago.

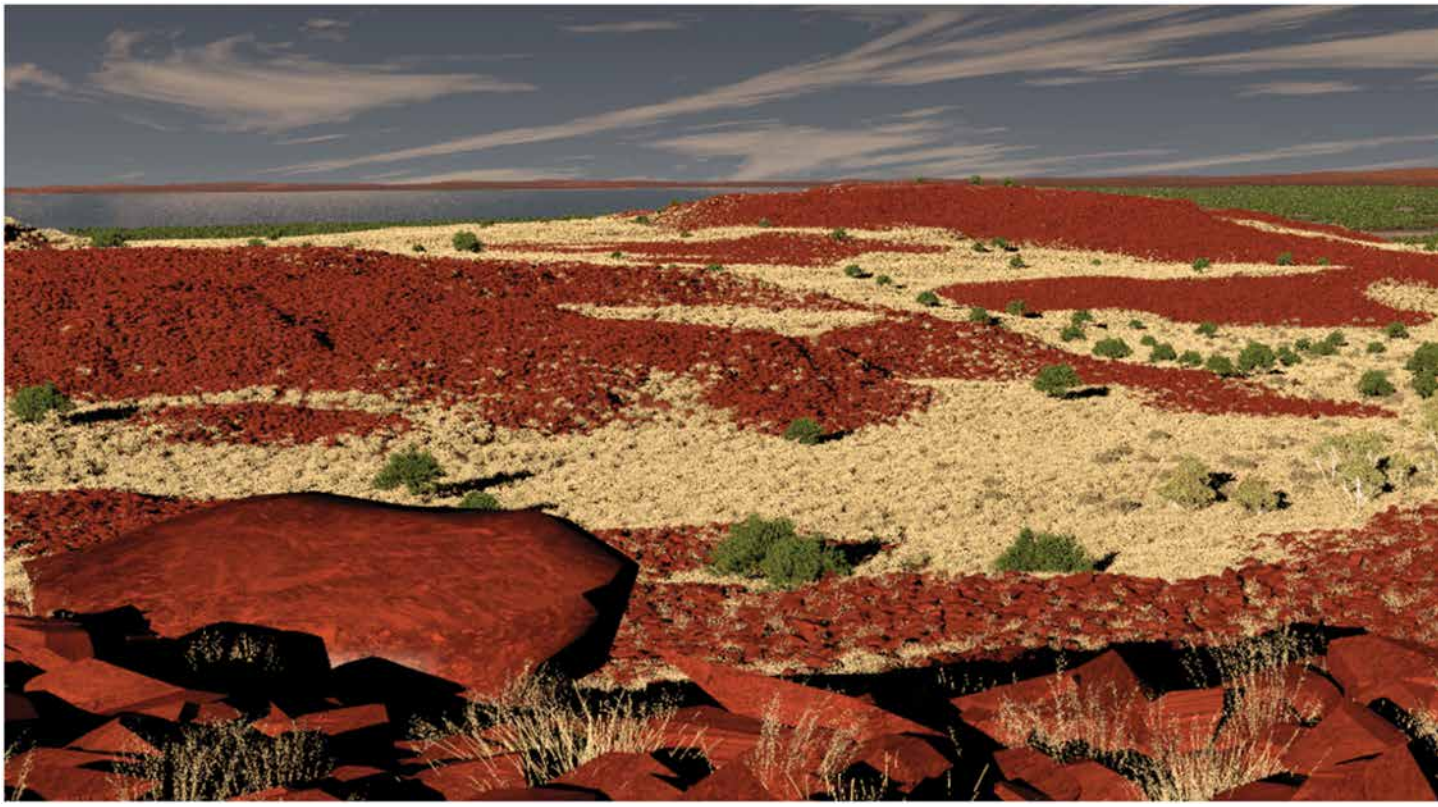

(Above) Figure 19.19. Ground-level visualisation offshore from modern Rosemary Island c. 1842.

(Below) Figure 19.20. Ground-level visualisation of the ridgeline on Murujuga c. 1868.

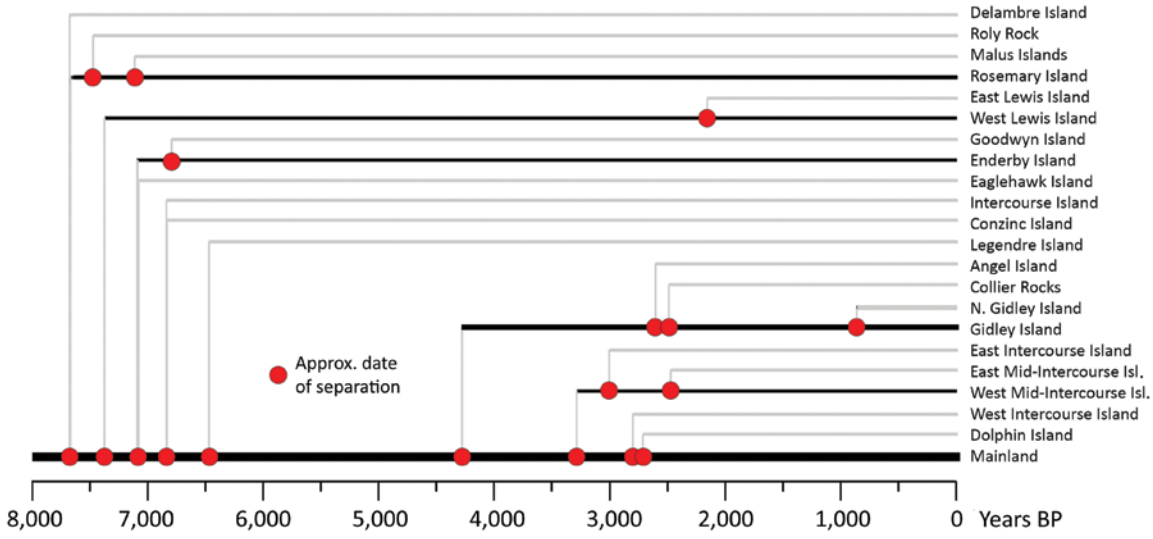

Figure 19.16. Islandisation in the Dampier Archipelago.

The ground-level visualisation of modern Rosemary Island at 4 kya offshore (Figure 19.17) shows the edge of the mangroves (*Avicennia marina*) extending across the shallow bay and protected from strong surf by an offshore reef located to the north-west. On the mainland, the distant shoreline is now in view, on the left (Figure 19.18). Mangroves are re-establishing themselves along the stabilising shoreline, but sparse spinifex and other grasses still dominate, with scattered Kanji bush and other mulgas. There is a small paperbark (*Melaleuca leucadendra*) in the right foreground.

Several specific events were used to illustrate the landscape as it appeared in the historic period. The arrival of the American whaler *Connecticut* at Rosemary Island in 1842 is shown in Figure 19.19. The dark shadows underneath the relatively calm surface are differential sediment layers and underwater vegetation, including seagrasses. A hawksbill turtle (*Eretmochelys imbricata*) swims towards the beach in the foreground.

The Murujuga ridgeline location is shown at the time of the Flying Foam Massacre (1868). The visualisation shows well-established and extensive mangroves at the edges of both shorelines along the low peninsula attaching Murujuga to the mainland (Figure 19.20). The coolibah trees are denser along the seasonal drainages leading into the mangroves. This camera position, while illustrating a much more stable landscape over 50,000 years than the other camera, shows the vegetation has gone through a series of dramatic changes over that time.

The sequence of sea-level rise after 10 kya is particularly interesting given how quickly vast areas became inundated. As sea level is rising vertically, it would affect some areas much more dramatically than others in the *horizontal* dimension. Knowing the locations and distributions of such areas could be very useful to understanding where people may have settled during specific periods in the past, and where currently inundated archaeological sites might have undergone limited or more extended periods of shoreline erosion. This can be seen to some degree in the animated visualisations.

To quantify the rapidity of this incursion, we examined the rate of horizontal shoreline loss as a function of the slope of the local terrain. This was done by creating a 'pseudo-topography' to compare against the actual terrain model. Depth contours were generated for every 100 years during the period between 10 kya and today. A surface was interpolated using the 'topo to raster' function in ArcGIS. The result is a terrain model where 'sea level' represents the modern shoreline and 'elevation' below that is not measured in metres, but in years. Each pixel contains a value which represents the number of years prior to 0 kya that the 'shoreline' passed through it, back 10 kya. The 'steepness' of this slope (Figure 19.21) represents the speed of sea-level rise.

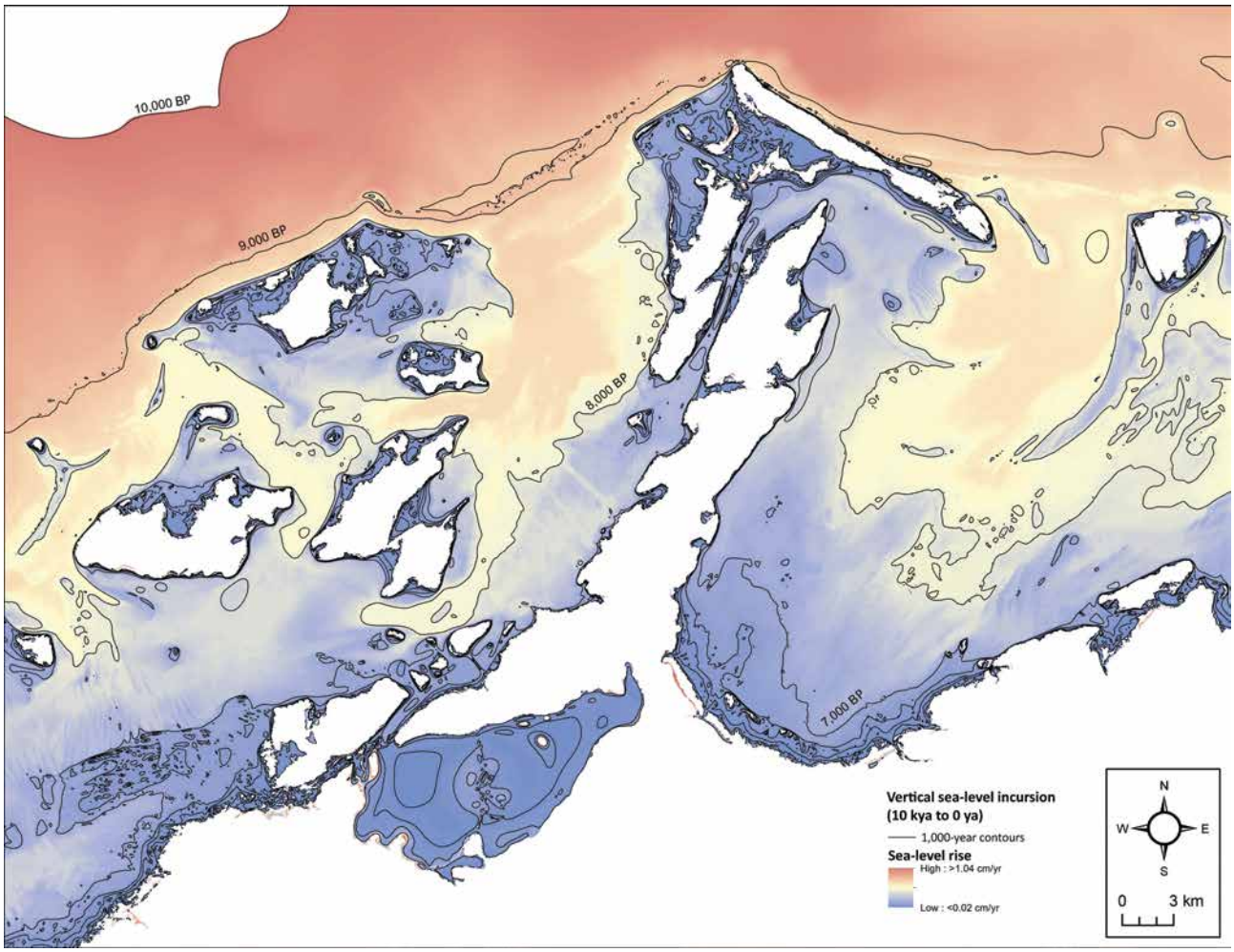

Figure 19.21. Shoreline stability of Murujuga: model of vertical sea-level rise (10 kya to 0 ya).

With each pixel having a horizontal extent of 30 m and a specific speed of sea-level rise, it is possible to convert that slope into the number of years that it took for the 'shoreline' to cross each pixel – that is, the rate of local horizontal inundation (Figure 19.22). What is notable in this image is the variable extent of the blue areas compared to Figure 19.21. These locations are where shorelines are likely to have been stable during this 10,000-year period of sea-level incursion. The last 5,000 years were the most stable along the entire sea–land interface. But even during periods of very rapid sea-level rise (from 10 kya to 7 kya), some areas such as those from Rosemary to Legendre islands, were experiencing little horizontal shoreline loss, even while other areas (in darker red) were losing more than 100 m of shoreline annually. At depths greater than 30 m here, resolution is lost as the 2021 digital elevation model data is replaced by the 2009 lower resolution data.

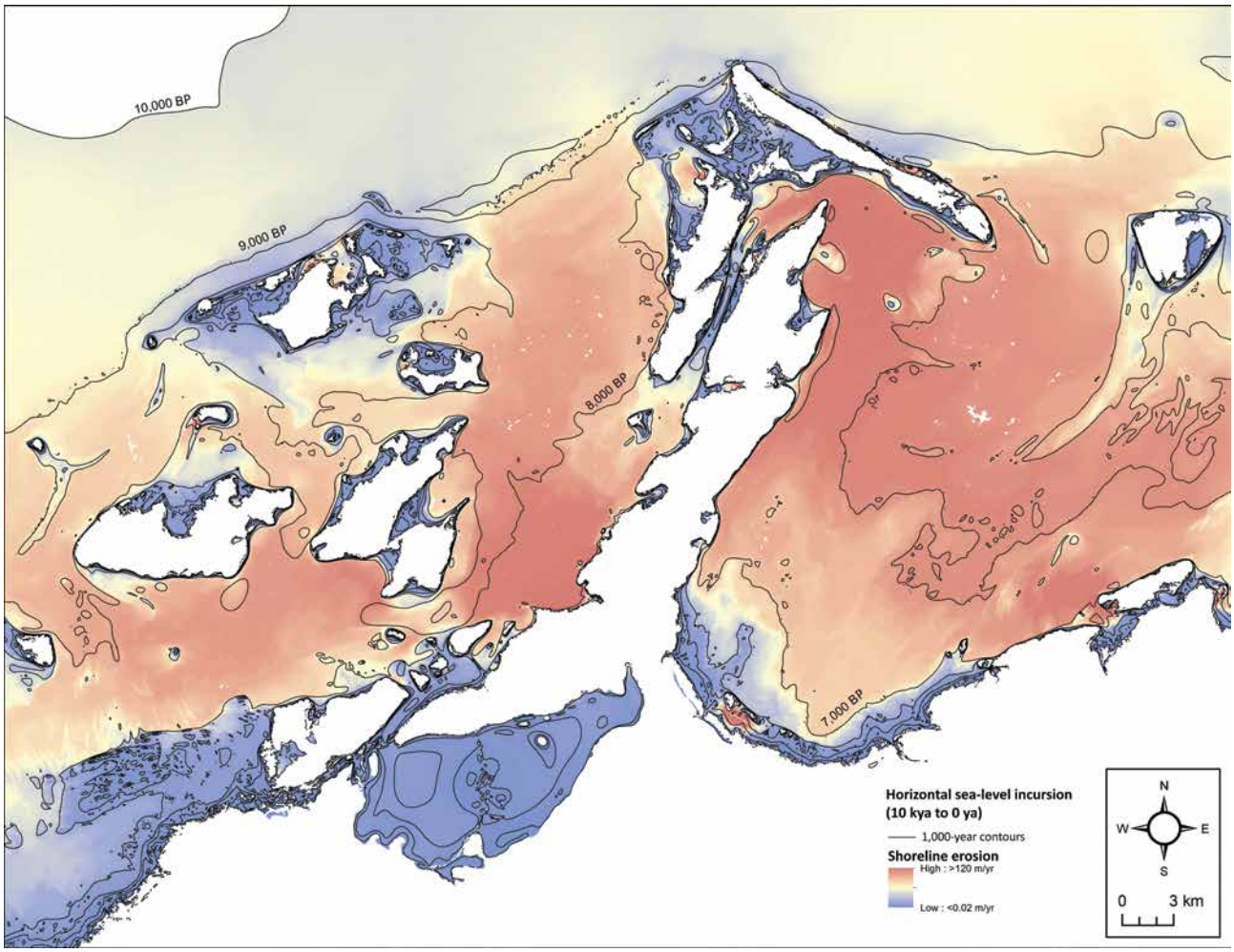

Figure 19.22. Shoreline stability of Murujuga: model of horizontal inundation (10 kya to 0 kya).

A rapid *vertical* sea-level rise alone may have dramatically limited the availability of littoral zone or reef-based resources. But resource adaptability is extremely complex and we have (as yet) a very limited understanding of the specific distribution of intensive maritime resource exploitation sites during this period. Access to stable shorelines would not only have provided the best resource base but allowed the best protection of archaeological sites from post-depositional erosion. The geomorphology is, again, a major factor. This simulation does not take into consideration the local complexity of the hydrodynamics and the effects it may have had on the terrain which preceded these modern surfaces, and stable shorelines may have been distributed differently than we can currently imagine. For that level of detail, more data is needed.

Conclusions

By combining the spatial analytical power of ArcGIS and the photorealistic visualisation tools available with Terragen, we can start to build dynamic visual models of the landscape and palaeoenvironment based on quantitative and qualitative data sources. These interpretations allow us to examine both large-scale processes and immersive 'snapshots' of the past. From these, we might interpret innovative ideas about past human settlement and adaptation.

Our low earth orbit animations of the last 125,000 years of landscape and environmental change at Murujuga demonstrate that our understanding of ancient shorelines based on sea-level models and bathymetry is still in its infancy. The animations indicate a wide range of potential shoreline dynamics despite inadequate local geomorphological evidence. Dramatic sea-level changes, in terms of the speed of inundation, have differentially affected Murujuga, particularly in the Holocene. Some areas were relatively stable over extended periods because of local slope and conditions. Such areas may have presented stable and productive opportunities for maritime resource foragers that were not available where shoreline migration was more dramatic. The verticality of sea-level rise or fall affects the nature of reef-build-

ing and littoral zone productivity. But horizontal stability could have ameliorated those effects, suggesting an environment much more amenable to maritime and coastal exploitation patterns, in deeper time, along certain landforms now submerged.

Our photorealistic visualisations at ground level during different time frames provide insights into how past people experienced their surroundings. Some areas are likely to have witnessed dramatic changes to the landscape over time; some much less so. We tend to view climatic conditions as regionally more uniform than they probably actually were, while micro-climatic and local variability was much greater than we might typically expect. Using this experimental perspective and developing these immersive visualisations demonstrates that some locations had persistent local terrain and landmarks over the many thousands of years of human occupation despite dramatic changes in vegetation. The granophyres, granites and gabbros of Murujuga have been characteristic of this landscape for more than 2 billion years and underlaid the many changing biotic communities. For past human occupants of this region, they formed persistent 'islands' in the interior long before they became actual islands offshore – a resilient canvas for rock art production through this area's human history.

References

Autodesk, Inc. 2022. *3ds Max*. <https://www.autodesk.com.au/products/3ds-max/overview>.

Benjamin, J., M. O'Leary, J. McDonald, C. Wiseman, J. McCarthy, E. Beckett, P. Morrison, F. Stankiewicz, J. Leach, J. Hacker. P. Baggaley et al. 2020. Aboriginal artefacts on the continental shelf reveal ancient drowned cultural landscapes in northwest Australia. *PloS One* 15(7): e0233912. https://doi.org/10.1371/journal.pone.0233912

BOM (Bureau of Meteorology). 2015. *Australian hydrological geospatial fabric (Geofabric): Version 3*. Commonwealth of Australia. <http://www.bom.gov.au/water/geofabric/>.

Bowler, J. M., G. A. T. Duller, N. Perret, J. Prescott and K.-H. Wyrwoll. 1998. Hydrologic changes in monsoonal climates of the last glacial cycle: stratigraphy and lumenescence dating of Lake Woods, NT, Australia. *Palaeoclimates* 3(1–3): 179–207.

Clarkson, C., Z. Jacobs, B. Marwick, R. Fullagar, L. Wallis, M. Smith, R. G. Roberts, E. Hayes, K. Lowe, X. Carah, S. A. Florin, J. McNeil, D. Cox, J. L. Arnold, Q. Hua, J. Huntley, H. E. A. Brand, T. Manne, A. Fairbairn, J. Shulmeister, L. Lyle, M. Salinas, M. Page, K. Connell, G. Park, K. Norman, T. Murphy and C. Pardoe. 2017. Human occupation of northern Australia by 65,000 years ago. *Nature* 547: 306–310. https://www.nature.com/articles/nature22968

Claussen, M., A. Ganopolski, V. Brovkin, F.-W. Gerstengarbe and P. Werner. 2003. Simulated global-scale response of the climate system to Dansgaard/Oeschger and Heinrich events. *Climate Dynamics* 21: 361–370. https://doi.org/10.1007/s00382-003-0336-2

Collins, L. B., J.-X. Zhao and H. Freeman. 2006. A high-precision record of mid–late Holocene Sea-level events from emergent coral pavements in the Houtman Abrolhos Islands, southwest Australia. *Quaternary International* 145–146: 78–85. https://doi.org/10.1016/j.quaint.2005.07.006

Collins, L. B., Z. R. Zhu, K.-H. Wyrwoll and A. Eisenhauer. 2003. Late quaternary structure and development of the northern Ningaloo Reef, Australia. *Sedimentary Geology* 159: 81–94. https://doi.org/10.1016/S0037-0738(03)00096-4

De Deckker, P., T. T. Barrows and J. Rogers. 2015. Land–sea correlations in the Australian region: post-glacial onset of the monsoon in northwestern Western Australia. *Quaternary Science Reviews* 105: 181–194. https://doi.org/10.1016/j.quascirev.2014.09.030

De Deckker, P., M. Moros, K. Perner, T. Blanz, L. Wacker, R. Schneider, T. T. Barrows, T. O'Loingsigh and E. Jansen. 2020. Climatic evolution in the Australian region over the last 94 ka –spanning human occupancy – and unveiling the last glacial maximum. *Quaternary Science Reviews* 249: 106593. https://doi.org/10.1016/j.quascirev.2020.106593

Denniston, R. F., K.-H. Wyrwoll, Y. Asmerom, V. J. Polyak, W. F. Humphreys, J. Cugley, D. Woods, Z. LaPointe, J. Peota and E. Greaves. 2013a. North Atlantic forcing of millennial-scale Indo-Australian monsoon dynamics during the last glacial period. *Quaternary Science Reviews* 72: 159–168. https://doi.org/10.1016/j.quascirev.2013.04.012

Denniston, R.F., K.-H. Wyrwoll, V. J. Polyak, J. R. Brown, Y. Asmerom, A. D. Wanamaker Jr, Z. LaPointe, R. Ellerbroek, M. Barthelmes, D. Cleary, J. Cugley, D. Woods and W. F. Humphreys. 2013b. A stalagmite record of Holocene Indonesian–Australian summer monsoon variability from the Australian tropics. *Quaternary Science Reviews* 78: 155–168. https://doi.org/10.1016/j.quascirev.2013.08.004

Esri (Environmental Systems Research Institute). 2021. *ArcGIS 10.8.1*. <https://www.esri.com/en-us/arcgis/about-arcgis/overview>.

Fitzsimmons, K. E., T. J. Cohen, P. P. Hesse, J. Jansen, G. C. Nanson, J.-H. May, T. T. Barrows, D. Haberlah, A. Hilgers, T. Kelly, J. Larsen, J. Lomax and P. Treble. 2013. Late quaternary palaeoenvironmental change in the Australian drylands. *Quaternary Science Reviews* 74: 78–96. https://doi.org/10.1016/j.quascirev.2012.09.007

Florabase. 2022. Western Australian Herbarium, Perth: Department of Biodiversity, Conservation and Attractions. <https://florabase.dpaw.wa.gov.au/>.

Gallant, J. C., N. Wilson, T. I. Dowling, A. M. Read and C. Inskeep. 2011. *SRTM-derived 1 second digital elevation models version 1.0*. Canberra: Geoscience Australia. <https://ecat.ga.gov.au/geonetwork/srv/eng/catalog.search#/metadata/72759>.

Ganopolski, A. and S. Rahmstorf. 2001. Rapid changes of glacial climate simulated in a coupled model. *Nature* 409: 153–158. https://www.nature.com/articles/35051500

M. L., R. N. Drysdale, M. K. Gagan, J.-X. Zhao, L. K. Ayliffe, J. C. Hellstron, W. S. Hantoro, S. Frisia, Y.-X. Feng, I. Cartwright, E. St Pierre, M. J. Fischer and B. W. Suwargadi. 2009. Increasing Australian–Indonesian monsoon rainfall linked to early Holocene sea-level rise. *Nature Geoscience* 2: 636–639. https://www.nature.com/articles/ngeo605

Hesse, P. P., J. W. Magee and S. van der Kaars. 2004. "Late quaternary climates of the Australian arid zone: a review. *Quaternary International* 118–119: 87–102. https://doi.org/10.1016/S1040-6182(03)00132-0

Hiscock, P. and L. A. Wallis. 2005. Pleistocene settlement of deserts from an Australian perspective. *Desert Peoples: Archaeological Perspectives*, eds P. Veth, M. Smith and P. Hiscock, pp. 34–57. Oxford: Wiley Blackwell. https://doi.org/10.1002/9780470774632.ch3

Holdaway, S., and P. Fanning. 2014. *Geoarchaeology of Aboriginal Landscapes in Semi-arid Australia*. Canberra: CSIRO Publishing.

Johnson, B. J., G. H. Miller, M. L. Fogel, J. W. Magee, M. K. Gagan and A. R. Chivas. 1999. 65,000 years of vegetation change in central Australia and the Australian summer

monsoon. *Science* 284: 1150–1152. https://doi.org/10.1126/science.284.5417.1

Jouzel, J., V. Masson-Delmotte, O. Cattani, G. Dreyfus, S. Falourd, G. Hoffmann, B. Minster, J. Nouet, J. M. Barnola, J. Chappellaz, H. Fischer, J. C. Gallet, S. Johnsen, M. Leuenberger, L. Loulergue, D. Luethi, H. Oerter, F. Parrenin, G. Raisbeck, D. Raynaud, A. Schilt, J. Schwander, E. Selmo, R. Souchez, R. Spahni, B. Stauffer, J. P. Steffensen, B. Stenni, T. F. Stocker, J. L. Tison, M. Werner and E. W. Wolff. 2007. Orbital and millennial Antarctic climate variability over the last 800,000 years. *Science* 317: 793–796. https://doi.org/10.1126/science.1141038

Kamperov, D. 2020. *Classic erosion* [software]. <https://daniilkamperov.com/>.

Lambeck, K., H. Rouby, A. Purcell, Y. Sun and M. Sambridge. 2014. Sea level and global ice volumes from the last glacial maximum to the Holocene. *Proceedings of the National Academy of Sciences* 111: 15296–15303. https://doi.org/10.1073/pnas.141176211

Larcombe, P., I. Ward and T. Whitley. 2018. Physical sedimentary controls on subtropical coastal and shelf sedimentary systems: initial application in conceptual models and computer visualisations to support archaeology. *Geoarchaeology* 33: 661–679. https://doi.org/10.1002/gea.21681

Lebrec, U., V. Paumard, M. J. O'Leary and S. C. Lang. 2021a. Towards a regional high-resolution bathymetry of the North West Shelf of Australia based on Sentinel-2 satellite images, 3D seismic surveys, and historical datasets. *Earth System Science Data: Open Access* 13: 5191–5212. https://doi.org/10.5194/essd-13-5191-2021

Lebrec, U., V. Paumard, M. J. O'Leary and S. C. Lang. 2021b. *High-resolution digital elevation model of the North West Shelf – 30m*. Canberra: Geoscience Australia. https://doi.org/10.26186/144600

McDonald, J., P. Veth, A. Paterson, J. Hampson, K. Glaskin, T. Whitley, P. Bourke and K. Mulvaney. 2013. *Murujuga – Dynamics of the Dreaming*. Canberra and Melbourne: Australian Research Council Linkage Projects and Rio Tinto.

McDonald, J., W. Reynen, K. Ditchfield, J. Dortch, M. Leopold, B. Stephenson, T. Whitley, I. Ward and P. Veth. 2018b. Murujuga Rockshelter: first evidence for Pleistocene occupation on the Burrup Peninsula. *Quaternary Science Reviews* 193: 266–287. https://doi.org/10.1016/j.quascirev.2018.06.002

McNiven, I. J., J. Crouch, J. M. Bowler, J. E. Sherwood, N. Dolby, J. E. Dunn and J. Stanisic. 2019. The Moyjil site, south-west Victoria, Australia: excavation of a last interglacial charcoal and burnt stone feature – is it a hearth? *Proceedings of the Royal Society of Victoria* 130: 94–116. https://doi.org/10.1071/RS18008

Magee, J. W. and G. H. Miller. 1998. Lake Eyre palaeohydrology from 60 ka to the present: beach ridges and glacial maximum aridity. *Palaeogeography, Palaeoclimatology, Palaeoecology* 144: 307–329. https://doi.org/10.1016/S0031-0182(98)00124-2

Mahowald, N. M., D. R. Muhs, S. Levis, P. J. Rasch, M. Yoshioka, C. S. Zender and C. Luo. 2006. Change in atmospheric mineral aerosols in response to climate: last glacial period, preindustrial, modern, and doubled carbon dioxide climates. *Journal of Geophysical Research: Atmospheres* 111(D10): 202. https://doi.org/10.1029/2005JD006653

Miller, G. H., J. Mangan, D. Pollard, S. L. Thompson, B. S. Felzer and J. W. Magee. 2005. Sensitivity of the Australian monsoon to insolation and vegetation: implications for human impact on continental moisture balance. *Geology* 33: 65–68. https://doi.org/10.1130/G21033.1

Mitchell, A.A., and D. G. Wilcox. 1994. *Arid Shrubland Plants of Western Australia*. Perth: University of Western Australia Press.

Moore, P. 2005. *A Guide to Plants of Inland Australia*. Sydney: New Holland.

NASA (National Aeronautics and Space Administration). 2022. *Shuttle radar topography mission*. <https://www2.jpl.nasa.gov/srtm/>.

NOAA (National Oceanic & Atmospheric Administration). 2022. *Solar position calculator*. <https://gml.noaa.gov/grad/solcalc/>.

O'Leary, M. J., P. J. Hearty, W. G. Thompson, M. E. Raymo, J. X. Mitrovica and J. M. Webster. 2013. Ice sheet collapse following a prolonged period of stable sea level during the last interglacial. *Nature Geoscience* 6: 796–800. https://www.nature.com/articles/ngeo1890

Petheram, R. J., and B. Kok. 2003. *Plants of the Kimberley Region of Western Australia*. Perth: University of Western Australia Press.

Petit, J. R., J. Jouzel, D. Raynaud, N. I. Barkov, J. M. Barnola, I. Basile, M. Bender, J. Chappellaz, M. Davis, G. Delaygue, M. Delmotte, V. M. Kotlyakov, M. Legrand, V. Y. Lipenkov, C. Lorius, L. Pepin, C. Ritz, E. Saltzman and M. Stievenard. 1999. Climate and atmospheric history of the past 420,000 years from the Vostok ice core, Antarctica. *Nature* 399: 429–436. https://www.nature.com/articles/20859

Planetside Software. 2022. *Terragen 4.6.11*. <http://planetside.co.uk/>.

Reeves, J. M., T. T. Barrows, T. J. Cohen, A. S. Kiem, H. C. Bostock, K. E. Fitzsimmons, J. D. Jansen, J. Kemph, C. Krause, L. Petherick, S. J. Phipps and OZ-INTIMATE Members. 2013. Climate variability over the last 35,000 years recorded in marine and terrestrial archives in the Australian region: an OZ-INTIMATE compilation. *Quaternary Science Reviews* 74: 21–34. https://doi.org/10.1016/j.quascirev.2013.01.001

Siddall, M., E. J. Rohling, A. Almogi-Labin, Ch. Hemleben, D. Meischner, I. Schmelzer and D. A. Smeed. 2003. Sea-level fluctuations during the last glacial cycle. *Nature* 423: 853–858. https://www.nature.com/articles/nature01690

Silva3D. No date. <https://www.silva3d.com/>

Skippington, J., T. Manne and P. Veth. 2021. Isotopic indications of late Pleistocene and Holocene paleoenvironmental changes at Boodie Cave archaeological site, Barrow Island, Western Australia. *Molecules* 26: 2582. https://doi.org/10.3390/molecules26092582

van der Kaars, S., and P. De Deckker. 2002. A late quaternary pollen record from deep-sea core Fr10/95, GC17 offshore Cape Range Peninsula, northwestern Western Australia. *Review of Palaeobotany and Palynology* 120: 17–39. https://doi.org/10.1016/S0034-6667(02)00075-1

van der Kaars, S., P. De Deckker and F. X. Gingele. 2006. A 100 000-year record of annual and seasonal rainfall and temperature for northwestern Australia based on a pollen record obtained offshore. *Journal of Quaternary Science* 21: 879–889. https://doi.org/10.1002/jqs.1010

Van Meerbeeck, C. J., H. Renssen and D. M. Rochel. 2009. How did marine isotope stage 3 and last glacial maximum climates differ? – perspectives from equilibrium simulations. *Climate of the Past* 5: 33–51. https://doi.org/10.5194/cp-5-33-2009

Vannieuwenhuyse, D., S. O'Connor and J. Balme. 2017. Settling in Sahul: investigating environmental and human history interactions through micromorphological analyses in tropical semi-arid north-west Australia. *Journal of Archaeological Science* 77: 172–193. https://doi.org/10.1016/j.jas.2016.01.017

van Osterzee, P. 2009. *A Field Guide to Central Australia*. Marleston, SA: Gecko Books.

Veth, P., I. Ward and K. Ditchfield. 2016a. Reconceptualising last glacial maximum discontinuities: a case study from the maritime deserts of north-western Australia. *Journal of Anthropological Archaeology* 46: 82–91. https://doi.org/10.1016/j.jaa.2016.07.016

Veth, P., I. Ward and T. Manne. 2016b. Coastal feasts: a Pleistocene antiquity for resource abundance in the maritime deserts of north west Australia? *Journal of Island and Coastal Archaeology* 12: 8–23. http://dx.doi.org/10.1080/15564894.2015.1132799

Veth, P., M. Smith, J. Bowler, K. Fitzsimmons, A. Williams and P. Hiscock. 2009. Excavations at Parnkupirti, Lake Gregory, Great Sandy Desert: OSL ages for occupation before the last glacial maximum. *Australian Archaeology* 69: 1–10. https://doi.org/10.1080/03122417.2009.11681896

Veth, P., K. Aplin, L. Wallis, T. Manne, T. Pulsford, E. White and A. Chappell. 2007. *The Archaeology of Montebello Islands, North-West Australia: Late Quaternary Foragers on an Arid Coastline*. Oxford: Archaeopress.

Veth, P., I. Ward, T. Manne, S. Ulm, K. Ditchfield, J. Dortch, F. Hook, F. Petchey, A. Hogg, D. Questiaux, M. Demuro, L. Arnold, N. Spooner, V. Levchenko, J. Skippington, C. Byrne, M. Basgall, D. Zeanah, D. Belton, P. Helmholz, S. Bajkan, R. Bailey, C. Placzek and P. Kendrick. 2017. Early human occupation of a maritime desert, Barrow Island, North-West Australia. *Quaternary Science Reviews* 168: 19–29. https://doi.org/10.1016/j.quascirev.2017.05.002

Waelbroeck, C., L. Labeyrie, E. Michel, J. C. Duplessy, J. F. McManus, K. Lambeck, E. Balbona and M. Labracherie. 2002. Sea-level and deep water temperature changes derived from benthic foraminifera isotopic records. *Quaternary Science Reviews* 21: 295–305. https://doi.org/10.1016/S0277-3791(01)00101-9

Ward, I., P. Larcombe and P. Veth. 2015. A new model for coastal resource productivity and sea-level change: the role of physical sedimentary processes in assessing the archaeological potential of submerged landscapes from the Northwest Australian Continental Shelf. *Geoarchaeology* 30: 19–31. https://doi.org/10.1002/gea.21498

Whiteway, T. 2009. *Australian bathymetry and topography grid, June 2009*. Canberra: Geoscience Australia. <https://ecat.ga.gov.au/geonetwork/srv/eng/catalog.search#/metadata/67703>.

Whitley, T. 2022. *New NW Australia 125k to today visualization – with sites* [video]. YouTube, 1 June. <https://www.youtube.com/watch?v=RCTqpcFHj34>.

Whitley, T., M. Berry and L. Clayton. 2018. Visualizing 125,000 years of environmental and landscape change in NW Australia. https://doi.org/10.13140/RG.2.2.19934.95042.

Williams, A. N., S. Ulm, A. R. Cook, M. C. Langley and M. Collard. 2013. Human refugia in Australia during the last glacial maximum and terminal Pleistocene: a geospatial analysis of the 25–12 ka Australian archaeological record. *Journal of Archaeological Science* 40: 4612–4625. https://doi.org/10.1016/j.jas.2013.06.015

Williams, A. N., P. Veth, W. Steffen, S. Ulm, C. S. M. Turney, J. M. Reeves, S. J. Phipps and M. Smith. 2015b. A continental narrative: human settlement patterns and Australian climate change over the last 35,000 years. *Quaternary Science Reviews* 123: 91–112. https://doi.org/10.1016/j.quascirev.2015.06.018

Wilson, B. 2013. *The Biogeography of the Australian North West Shelf: Environmental Change and Life's Response*. Burlington, MA: Elsevier.

Wilson, O., M. Spinoccia and C. Buchanan. 2012. *50m multibeam dataset of Australia 2012*. Canberra: Geoscience Australia. <https://ecat.ga.gov.au/geonetwork/srv/eng/catalog.search#/metadata/73842>.

Woodroffe, C. D., and J. M. Webster. 2014. Coral reefs and sea-level change. *Marine Geology* 352: 248–267. https://doi.org/10.1016/j.margeo.2013.12.006

Wyrwoll, K.-H., and G. H. Miller. 2001. Initiation of the Australian summer monsoon 14,000 years ago. *Quaternary International* 83–85: 119–128. https://doi.org/10.1016/S1040-6182(01)00034-9

Xfrog. 2022. <http://xfrog.com/>.

Yokoyama, Y., P. De Deckker, K. Lambeck, P. Johnston and L. K. Fifield. 2001. Sea-level at the last glacial maximum: evidence from northwestern Australia to constrain ice volumes for oxygen isotope stage 2. *Palaeogeography, Palaeoclimatology, Palaeoecology* 165: 281–297. https://doi.org/10.1016/S0031-0182(00)00164-4.

First published in 2023 by
UWA Publishing
Crawley, Western Australia 6009
www.uwap.uwa.edu.au
UWAP is an imprint of UWA Publishing,
a division of The University of Western Australia.

ISBN: 978-1-76080-253-0
Design by Upside Creative.